

# Lanczos, the transfer matrix, and the signal-to-noise problem

Michael L. Wagman<sup>1</sup>

<sup>1</sup>*Fermi National Accelerator Laboratory, Batavia, IL 60510, USA*

This work introduces a method for determining the energy spectrum of lattice quantum chromodynamics (LQCD) by applying the Lanczos algorithm to the transfer matrix. Proof-of-principle analyses of the simple harmonic oscillator and the LQCD proton mass demonstrate that this method provides faster ground-state convergence than standard energy estimators, which are related to the power-iteration algorithm. Lanczos provides more accurate energy estimates than multi-state fits to correlation functions with small imaginary times while achieving comparable statistical precision. Two-sided error bounds are computed for Lanczos results and guarantee that excited-state effects cannot shift Lanczos results far outside their statistical uncertainties. Further, Lanczos results avoid the exponential signal-to-noise degradation present in standard energy estimators.

Determining the energy spectrum of quantum chromodynamics (QCD) leads to hadron mass predictions and is an essential first step towards predicting hadron and nuclear structure, scattering amplitudes, and inputs to new physics searches. Spectroscopy, the determination of ground- and excited-state energies, is therefore a central aspect of lattice QCD (LQCD) calculations. Accurately disentangling ground- and excited-state effects is challenging for systems with small energy gaps and leads to significant and hard-to-quantify uncertainties in state-of-the-art LQCD calculations for example of nucleon axial form factors [1–8] and baryon-baryon scattering [9–13].

Spectroscopy calculations typically rely on analyzing the asymptotic decay rate of Euclidean correlation functions, which is set by the lowest-energy state not orthogonal to those created by the relevant operators. However, the signal-to-noise (StN) ratios of Euclidean correlation functions also decay exponentially in Euclidean time with a rate predicted by Parisi and Lepage [14, 15]. This so-called StN problem is a major challenge for proton and other baryon correlation functions and becomes exponentially more severe for nuclei [16–18].

The StN problem has motivated the development of methods to maximize the information that can be extracted from relatively precise correlation functions with small imaginary times. Techniques based on solving a generalized eigenvalue problem (GEVP) constructed from a symmetric correlation-function matrix provide both faster convergence and rigorous variational upper bounds on energies [19–23], and their application has become standard in LQCD spectroscopy for multi-hadron systems with small energy gaps [24–26]. Prony’s method for signal processing has also been applied to LQCD and shown to improve ground-state convergence [27–29].

This work proposes a new approach to LQCD spectroscopy using the Lanczos algorithm [30] to compute eigenvalues of the transfer matrix. The Lanczos algorithm has been widely applied for decades to computational linear algebra [31–36], quantum Monte Carlo calculations [37–39], and analysis of Dirac matrices in LQCD [40–43]. It provides a rapidly convergent method for computing eigenvalues of large matrices [44–47]. However, direct application of the Lanczos algorithm to the

LQCD transfer matrix is challenging because the transfer matrix is infinite-dimensional [48] and not directly constructed in path-integral Monte Carlo calculations.

Here, I show that the Lanczos algorithm can be applied to the LQCD transfer matrix using recursive formulae whose inputs are simply Euclidean correlation functions. The Kaniel-Paige-Saad (KPS) bound [44–46] implies that Lanczos energies converge exponentially faster than standard estimators near the continuum limit. Lanczos approximation errors can be estimated directly and provide two-sided error bounds, improving upon the one-sided variational bounds provided by GEVP solutions.

Further, Lanczos results do not suffer from exponential StN degradation with Parisi-Lepage scaling. An explanation for this behavior is proposed based on identifying Lanczos results with numerical approximations to the transfer-matrix projection operator solution to the StN problem proposed by Della Morte and Giusti [49–51]. Proof-of-principle results are shown for a quantum simple harmonic oscillator (SHO) and the proton mass in LQCD with close-to-physical quark masses.

**Method:** Lattice field theories do not have a continuous time-translation symmetry to be used to directly define a Hamiltonian operator  $H$ . The presence of discrete time-translation symmetry,  $t \rightarrow t + a$  where  $a$  is the lattice spacing, does allow a transfer matrix  $T = e^{-aH}$  to be defined that acts as an imaginary-time evolution operator. The transfer matrix for LQCD with the Wilson gauge and fermion actions has been explicitly constructed as a Hilbert-space operator and shown to be Hermitian and positive-definite [52]. A transfer matrix can also be constructed for theories with improved actions that acts as a positive-definite operator for low-energy states [53].

Euclidean correlation functions for a theory with temporal extent (inverse temperature)  $\beta$  and “interpolating operators”  $\psi$  and  $\psi^\dagger$  are matrix elements of powers of  $T$ ,

$$C(t) \equiv \langle \psi(t) \psi^\dagger(0) \rangle = \langle \psi | T^{t/a} | \psi \rangle + \dots, \quad (1)$$

where  $|\psi\rangle \equiv \psi^\dagger |0\rangle$  with  $|0\rangle$  the vacuum state and  $\dots$  denotes exponentially-suppressed thermal effects detailed in the Supplemental Material. Inserting complete sets of transfer-matrix eigenstates  $\sum_n |n\rangle \langle n|$  leads to the spec-

tral representation

$$C(t) = \sum_n \lambda_n \langle \psi | n \rangle \langle n | \psi \rangle = \sum_{n=0}^{\infty} |Z_n|^2 e^{-E_n t}, \quad (2)$$

where  $Z_n \equiv \langle n | \psi \rangle$  are overlap factors and energies are defined by  $E_n \equiv -(1/a) \ln \lambda_n$  in terms of transfer matrix eigenvalues  $\lambda_n \equiv \langle n | T | n \rangle$  in the sector with quantum numbers of  $\psi^\dagger | 0 \rangle$  ordered such that  $\lambda_0 \geq \lambda_1 \geq \dots$ . For large  $t$ , correlation functions are therefore dominated by contributions from the lowest-energy state that is not orthogonal to  $|\psi\rangle$ . The “effective mass” provides a standard estimator for the ground-state energy

$$E(t) \equiv -\frac{1}{a} \ln \left[ \frac{C(t)}{C(t-a)} \right] = E_0 + O\left(e^{-(t/a)\delta}\right), \quad (3)$$

where  $\delta \equiv a(E_1 - E_0)$  is the excitation gap.

Estimating the ground-state energy using the effective mass can be viewed as an application of the power-iteration method [54] to the transfer matrix as follows. This method defines  $|b_k\rangle \equiv T|b_{k-1}\rangle / \|T|b_{k-1}\rangle\|$  with  $|b_1\rangle = |\psi\rangle / \sqrt{\langle \psi | \psi \rangle}$ , which leads to  $|b_k\rangle \propto T^{k-1} |\psi\rangle$ . The largest eigenvalue of  $T$  is then approximated as

$$\mu_k \equiv \frac{\langle b_k | T | b_k \rangle}{\langle b_k | b_k \rangle} = \frac{\langle \psi | T^{2k-1} | \psi \rangle}{\langle \psi | T^{2(k-1)} | \psi \rangle} = \frac{C((2k-1)a)}{C((2k-2)a)}. \quad (4)$$

Taking the log gives the power-iteration energy estimate after  $k$  iterations:  $-(1/a) \ln \mu_k$ . This estimate is identical to the effective mass with  $t/a = 2k - 1$ .

The Lanczos algorithm [30] is widely appreciated to be superior to the power-iteration method for the task of approximating the largest eigenvalue of a matrix [31–35, 55, 56]. Both methods involve the Krylov space

$$\mathcal{K}^{(m)} = \text{span}\{|\psi\rangle, T|\psi\rangle, \dots, T^m|\psi\rangle\}, \quad (5)$$

and the approximation of eigenvectors as elements of  $\mathcal{K}^{(m)}$ . However, the Lanczos algorithm enables the explicit diagonalization of a Krylov-space approximation to  $T$  that leads to faster convergence as discussed below. Extremal eigenvalues, that is eigenvalues near regions of relatively low spectral density, of large matrices are often well-approximated by the Lanczos algorithm after 10s of iterations [47, 57, 58].

Defining an initial vector  $|v_1\rangle \equiv |\psi\rangle / \sqrt{\langle \psi | \psi \rangle}$ , the first step of the Lanczos algorithm is to compute  $\alpha_1 \equiv \langle v_1 | T | v_1 \rangle$  and the residual vector  $|r_2\rangle \equiv (T - \alpha_1) |v_1\rangle$ . Subsequent steps proceed by computing the residual norm  $\beta_j \equiv \sqrt{|\langle r_j | r_j \rangle|}$ , the next Lanczos vector  $|v_j\rangle \equiv |r_j\rangle / \beta_j$ , its matrix element  $\alpha_j \equiv \langle v_j | T | v_j \rangle$ , and the next residual  $|r_{j+1}\rangle \equiv (T - \alpha_j) |v_j\rangle - \beta_j |v_{j-1}\rangle$ . This can be summarized by the three-term recurrence

$$T |v_j\rangle = \alpha_j |v_j\rangle + \beta_j |v_{j-1}\rangle + \beta_{j+1} |v_{j+1}\rangle. \quad (6)$$

The resulting Lanczos vectors  $|v_j\rangle$  are orthonormal,  $\langle v_i | v_j \rangle = \delta_{ij}$ . The matrix elements of  $T$  in the Lanczos-vector basis,  $T_{ij}^{(m)} \equiv \langle v_i | T | v_j \rangle$ , form a tridiagonal matrix by Eq. (6). Its eigenvalues, denoted  $\lambda_n^{(m)}$  and often

called Ritz values, provide optimal Krylov-space approximations to eigenvalues of  $T$  [44–46].

The LQCD transfer matrix is an infinite-dimensional integral operator that cannot be explicitly represented numerically without some form of Hilbert-space truncation. However, the elements of  $T_{ij}^{(m)}$  are scalars constructed from inner products involving  $|\psi\rangle$  and  $T$ . The path integral definitions of  $T_{ij}^{(m)}$  can be related to those for Euclidean correlation functions  $C(ka)$  using recursion relations involving  $F_j^k \equiv \langle v_j | T^k | v_j \rangle$  and  $G_j^k \equiv \langle v_j | T^k | v_{j-1} \rangle$  presented in the Supplemental Material.<sup>1</sup> These provide the tridiagonal matrix elements  $T_{ij}^{(m)}$ , which can be diagonalized to provide  $\lambda_k^{(m)}$  and  $E_k^{(m)} \equiv -(1/a) \ln \lambda_k^{(m)}$ .

**Convergence:** Cauchy’s interlacing theorem guarantees that  $\lambda_k^{(m)}$  provides a lower bound on  $\lambda_k$  [45, 60]. Therefore  $E_k^{(m)}$  provides a variational upper bound on  $E_k$ . The KPS bound [44–46] further constrains the approximation errors of ground-state Ritz values as detailed in the Supplemental Material:

$$\frac{\lambda_0^{(m)} - \lambda_0}{\lambda_0} \leq \left[ \frac{\tan \arccos Z_0}{T_{m-1}(2e^\delta - 1)} \right]^2, \quad (7)$$

where the  $T_k(x)$  are Chebyshev polynomials of the first kind,  $T_k(\cos x) = \cos(kx)$ . For large  $k$ ,  $T_k(x) \approx \frac{1}{2}(x + \sqrt{x^2 - 1})^k$ , and the KPS bound simplifies to

$$\frac{\lambda_0^{(m)} - \lambda_0}{\lambda_0} \lesssim \frac{4(1 - Z_0^2)}{Z_0^2} \times \begin{cases} e^{-2(m-1)\delta} & \delta \gg 1 \\ e^{-4(m-1)\sqrt{\delta}} & \delta \ll 1 \end{cases}. \quad (8)$$

For large  $\delta$ , this resembles the  $O(e^{-(t/a)\delta})$  asymptotic error of the effective mass (power-iteration method) with  $t/a \propto 2m$ . For small  $\delta$ , Lanczos converges exponentially faster than the power-iteration method because  $\sqrt{\delta} \gg \delta$ . The latter region is the relevant one near the continuum limit where  $\delta = a(E_1 - E_0) \ll 1$ .

Fig. 1 compares the practical convergence of  $E_0^{(m)}$  with that of  $E(t)$  as well as an improved estimator based on Prony’s method [27–29] for a 20-state correlation-function model defined by Eq. (2) with  $Z_n = (n+1)$  and  $aE_n = 0.1(n+1)$  for  $n = 0, \dots, 19$ . Both Lanczos and Prony results exactly determine the complete spectrum after 20 iterations. Prony’s method has the smallest error after 2–5 iterations, but its error subsequently increases and fluctuates. Lanczos converges monotonically to the exact result and is 5 orders of magnitude more accurate than either of the other methods after 12 iterations.

Remarkably, it is also possible to bound the difference between  $E_k^{(m)}$  and an exact energy in terms of directly calculable quantities [32, 45]. The approximation error

<sup>1</sup> Analogous recursion relations at the level of matrix elements have been discussed for Monte Carlo thermalization times in Ref. [59].

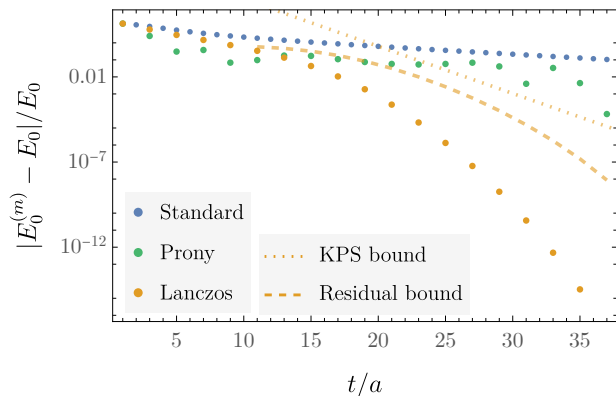


FIG. 1. Differences between the exact ground-state energy and the standard effective mass (blue), an estimator based on Prony’s method (green), and the Lanczos estimator  $E_0^{(m)}$  (orange) for the 20-state mock data described in the main text. Lanczos and Prony estimators with  $m$  iterations both involve  $C(0), \dots, C((2m-1)a)$  and are shown at  $t/a = 2m-1$ . The Kaniel-Paige-Saad bound, Eq. (7), is shown as a dotted line. The residual bound, Eq. (9), is shown as a dashed line for  $m \geq 6$  ( $E_0^{(m)}$  is closer to  $E_n$  with  $n > 0$  for smaller  $m$ ).

of  $T$  in the Lanczos basis is the residual norm  $\beta_{m+1}$  by Eq. (6), and the change of basis relating this to the Ritz basis is provided by the eigenvectors  $s_n^{(m)}$  of  $T_{ij}^{(m)}$ . The residual bound states that for any Ritz value  $\lambda_k^{(m)}$  there exists an eigenvalue  $\lambda$  of  $T$  whose distance from  $\lambda_k^{(m)}$  is within a two-sided window [32, 45, 61]:

$$\min_{\lambda \in \{\lambda_n\}} |\lambda_k^{(m)} - \lambda|^2 \leq \beta_{m+1}^2 |s_{mk}^{(m)}|^2, \quad (9)$$

where  $s_{jk}^{(m)}$  denotes the  $j$ -th component of  $s_k^{(m)}$ . Note that it is not guaranteed that  $\lambda_k^{(m)}$  is close to  $\lambda_k$  — eigenvectors that have sufficiently small overlap with  $|\psi\rangle$  can be “missed” by Lanczos [57, 58] — but a two-sided systematic uncertainty interval in which an eigenvalue of  $T$  is guaranteed to exist can be computed for each  $\lambda_k^{(m)}$ . This is a significant advantage over standard methods, which can also miss energy eigenstates in practice [11, 62–64] and for finite  $t$  only have one-sided systematic uncertainty bounds arising from the variational principle.

**Numerical Stability:** Numerical artifacts arising in the Lanczos algorithm from finite-precision arithmetic have been studied in detail and result in the appearance of “spurious eigenvalues” that do not converge towards definite values as well as multiple copies of genuine eigenvalues [45, 46, 61, 65–68]. A simple yet effective [40, 69] method for detecting and removing spurious eigenvalues was introduced by Cullum and Willoughby [65, 66]. This method is based on the non-trivial realization that large differences between Ritz values and  $T$  eigenvalues can only arise for a non-degenerate eigenvalue when  $\lambda_n^{(m)}$  is also an eigenvalue of the matrix  $\tilde{T}_{ij}^{(m)}$  defined by deleting

the first row and column of  $T_{ij}^{(m)}$  [65, 66].

The threshold for when eigenvalues of  $T_{ij}^{(m)}$  and  $\tilde{T}_{ij}^{(m)}$  should be considered identical — and thus spurious — is obvious in fixed-precision Lanczos applications without statistical noise [65, 66], but for Monte Carlo results it depends on statistical precision. Since spurious eigenvalues appear because of statistical fluctuations and do not converge to definite values, the Ritz value distribution obtained using bootstrap resampling [70–73] is useful for identifying spurious eigenvalues. A procedure for defining a threshold for the Cullum-Willoughby test based on bootstrap histograms is detailed in the Supplemental Material.

Non-spurious eigenvalues with  $\beta_j^2 \approx 0$  indicate that  $\lambda_j^{(m)}$  has converged to an eigenvalue of  $T$  within noise, see Eq. (9) and Refs. [32, 45, 61]. After convergence has been achieved, statistical fluctuations can easily lead to  $\beta_j^2 < 0$  and therefore complex  $T_{ij}^{(m)}$ . In this case, results can still be meaningfully interpreted in the context of an oblique Lanczos algorithm [67, 68, 74] in which matrix elements  $\langle w_j | T | v_j \rangle$  are computed between distinct bases of left- and right-Lanczos vectors. Assuming  $T$  is Hermitian (although  $T^{(k)}$  is non-Hermitian), the resulting Ritz values are identical to those obtained by naively applying symmetric Lanczos with  $\beta_j \in \mathbb{C}$ . The residual bound includes an additional ratio of Lanczos-vector and Ritz-vector norms, which are both equal to unity when  $T_{ij}^{(k)}$  is Hermitian; see the Supplemental Material.

**Simple harmonic oscillator:** Complex scalar field theory in  $(0+1)D$  with periodic boundary conditions,  $\varphi(\beta) = \varphi(0)$ , and action

$$S = a \sum_{t=0}^{\beta-1} \left\{ \varphi(t)^* [\varphi(t+a) - 2\varphi(t) + \varphi(t-a)] \frac{1}{a^2} + (aM)^2 |\varphi(t)|^2 \right\}, \quad (10)$$

describes a system of non-interacting bosons with mass  $aM$  at temperature  $1/\beta$ . For  $\beta \rightarrow \infty$  it is equivalent to a pair of simple harmonic oscillators. The theory has a  $U(1)$  symmetry  $\varphi \rightarrow e^{i\theta} \varphi$  whose conserved charge  $Q$  corresponds to  $\varphi$  particle number. Correlation functions for systems with charge  $Q$  have ground-state energies  $Qm$ . Since  $|\varphi|^2$  has  $Q = 0$ , the variances of charge  $Q$  correlation functions are asymptotically constant. This gives calculations of  $Q = 1$  correlation functions an exponentially severe StN problem that is similar to the StN problem facing baryons in LQCD [75, 76].

A correlation function with  $Q = 1$  that has overlap with both ground and excited states can be defined as

$$C_\varphi(t) \equiv \left\langle \varphi(t) |\varphi(t)|^{3/2} \varphi(0)^* |\varphi(0)|^{3/2} \right\rangle. \quad (11)$$

Results for  $E(t)$  and  $E_0^{(m)}$  are shown in Fig. 2 for a Monte Carlo ensemble of  $10^4$  field configurations with  $aM = 0.1$  and  $\beta/a = 100$  where  $C_\varphi(t)$  is averaged over

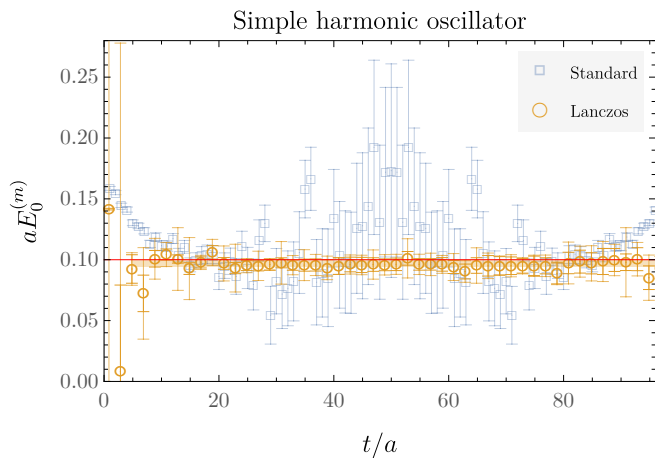


FIG. 2. The (thermal) effective mass  $\text{arccosh}([C(t+2a) + C(t)]/C(t+a))$  for a (0+1)D scalar compared with  $E_0^{(m)}$  for  $m = t/(2a) + 1/2$  Lanczos iterations. The red line shows the exact result  $E_0 = 0.1$ . Blue and inner orange error bars show bootstrap 68% confidence intervals, outer orange error bars include the (bootstrap median) residual added in quadrature, and the shaded orange region shows the 68% confidence interval of a fit to  $E_0^{(m)}$ .

all translations of the origin. Lanczos results converge within uncertainties to the true ground-state energy after  $m = 3$  iterations, corresponding to  $t/a = 5$ , while  $E(t)$  reaches similar convergence for  $t/a \sim 10$ . Further,  $E_0^{(m)}$  converges to the true ground-state energy even in the presence of thermal states, as proven in the Supplemental Material, and Lanczos results remain consistent with  $aM$  for  $t > \beta/2$ . The statistical precision of  $E_0^{(m)}$  also depends on  $t/a$  (via  $m = t/(2a) + 1/2$ ) very differently than the precision of  $E(t)$  — Lanczos results do not show exponential StN degradation with Parisi-Lepage scaling.

A constant fit to  $E_0^{(m)}$  starting when Lanczos results have converged within noise as defined in the Supplemental Material,  $t/a = 5$ , gives  $aE_0^{\text{Lanczos}} = 0.0972(31)$ . This can be compared to standard multi-state fits to  $C_\varphi(t)$  using the methodology detailed in Refs. [11, 77]: a two-state fit with the same minimum  $t/a = 5$  gives  $aE_0^{2\text{-state}} = 0.0933(39)$ , and a weighted average of multi-state fits with all minimum  $t/a$  choices gives  $aE_0^{\text{averaged}} = 0.0981(35)$ . Two-state fit results are  $1.7\sigma$  lower than the exact result  $aE_0 = 0.1$ , while Lanczos and model-averaged multi-state fit results both agree with  $aM$  within  $1\sigma$ . The corresponding Lanczos residual fit implies a SHO energy  $E$  satisfies  $a^2|E - E_0^{\text{Lanczos}}|^2 < 0.0001(40)$ .

**Lattice QCD:** Correlation functions for baryons and nuclei in LQCD have exponential StN problems that can make it difficult to isolate ground states using standard methods and are natural targets for applying Lanczos. To test the accuracy and precision of Lanczos methods for baryons with StN problems, I computed proton correlation functions  $C_p(t) = \langle p(t)\bar{p}(0) \rangle$  using point-like proton interpolating operators  $p(x) = u^T(x)C\gamma_5 d(x)(1+\gamma_4)d(x)$

projected to zero spatial momentum for 64 sources on each of 76 gauge-field configurations with  $L/a = 48$ ,  $\beta/a = 96$ , and  $N_f = 2 + 1$  dynamical quarks with approximately physical quark masses corresponding to  $m_\pi \approx 170$  MeV and  $a \approx 0.091(1)$  fm [78, 79]. The action corresponds to the Lüscher-Weisz gauge action [80] and clover-improved [81] Wilson fermion action with one step of stout smearing [82]; a Hermitian transfer matrix representation is therefore only valid for low-energy states [53].

Lanczos results shown in Fig. 3 are computed from correlation functions as above; see the Supplemental Material for more details including spurious eigenvalue distributions for proton (and analogous pion) correlation function results. A constant fit to  $E_0^{(m)}$  starting when Lanczos results have converged within noise,  $t/a = 11$ , gives  $aM_N^{\text{Lanczos}} = 0.433(11)$ . Two-state fits to  $C_p(t)$  with the same minimum  $t/a = 11$  give  $aM_N^{2\text{-state}} = 0.4383(86)$ . A weighted average of multi-state fits gives  $aM_N^{\text{averaged}} = 0.443(12)$ . For comparison, a standard analysis of a much larger statistical ensemble of 512 Gaussian-smear sources computed on  $N_{\text{cfg}} = 670$  gauge-field configurations with the same action computed by the NPLQCD Collaboration provides a high-precision benchmark:  $aM_N^{\text{big}} = 0.4244(44)$ . Two-state and model-averaged multi-state fit results are  $1.5\sigma$  and  $1.6\sigma$  larger than  $aM_N^{\text{big}}$ , respectively, while Lanczos results agree with  $aM_N^{\text{big}}$  within  $1\sigma$ . Fits to Lanczos residuals over the same range imply a LQCD energy  $E$  satisfies  $a^2|E - M_N^{\text{Lanczos}}|^2 < 0.0004(67)$ .

The variance of  $E_0^{(m)}$  is shown in Fig. 3 including uncertainties estimated using nested bootstrap resampling. Lanczos results have larger variance than standard results for relatively small  $t/a$ . However, the Lanczos variance is independent of  $t/a$  for  $15 \lesssim t/a \leq 96$ . One might worry that this is an artifact of correlations between Lanczos results arising from  $C(t)$  with all  $t/a \in \{0, \dots, 2m-1\}$  entering  $E_0^{(m)}$ ; however, the correlations  $\text{Corr}[E_0^{(m)}, E_0^{(m')}]$  are observed to decay with  $|m - m'|$  at a similar rate to those of  $\text{Corr}[E(2m-1), E(2m'-1)]$  as shown in the Supplemental Material.

**Discussion:** The method for applying the Lanczos algorithm to infinite-dimensional transfer matrices introduced here provides accurate predictions for simple harmonic oscillator and LQCD ground-state energies. In particular, Lanczos achieves higher accuracy and similar precision to multi-state fits involving small imaginary times. A two-sided error bound further shows excited-state effects cannot shift Lanczos results far outside their statistical uncertainties, although this residual bound is noisier than the energy results themselves. Challenges arise from spurious eigenvalues, but an implementation of the Cullum-Willoughby test using bootstrap histograms is sufficient to remove spurious eigenvalues in these examples. Future refinements improving the robustness of spurious eigenvalue removal could improve the statistical precision of Lanczos energy results and residual bounds.

The exponential StN degradation predicted by Parisi-

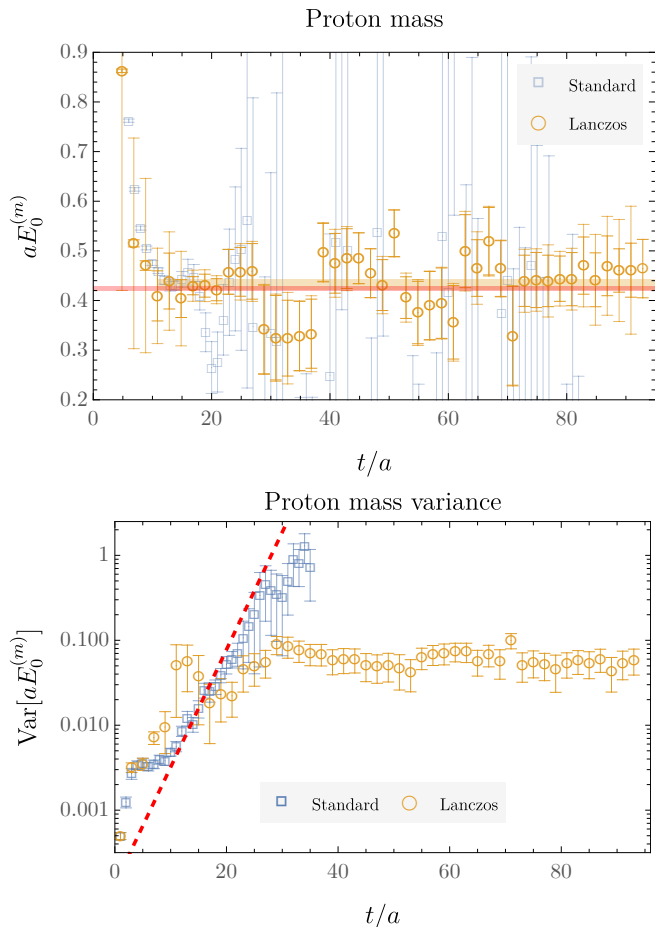


FIG. 3. Top,  $E(t)$  and  $E_0^{(m)}$  for the proton; details are as in Fig. 2. Bottom, the corresponding variances compared with Parisi-Lepage scaling  $\propto e^{(M_N - \frac{3}{2}m_\pi)t}$  (red dashed line).

Lepage scaling is absent from Lanczos SHO and LQCD results. A possible explanation is provided by analogy to the projection-operator solution to StN problems proposed by Della Morte and Giusti [49–51]. If a correlation function  $\langle \mathcal{O}(t)\bar{\mathcal{O}}(0) \rangle$  is replaced by  $\langle \mathcal{O}(t)P\bar{\mathcal{O}}(0) \rangle$  where  $P$  is a projection operator that selects a sector of Hilbert space with non-vacuum quantum numbers such as parity,  $U(1)$  charge, or baryon number, then only states with  $[\mathcal{O}(t)P\bar{\mathcal{O}}(0)][\bar{\mathcal{O}}(t)P^\dagger\mathcal{O}(0)]$  quantum numbers contribute to the variance. For the proton this corresponds to removing baryon-number-zero variance contributions from multi-pion states and leaving nucleon-antinucleon states.

The Lanczos algorithm can be characterized as a Krylov-space projection method [46, 74]. Explicitly, projection operators can be constructed from the Ritz vectors  $|y_n^{(m)}\rangle \equiv \sum_j |v_j^{(m)}\rangle s_{jn}^{(m)}$  as  $P_n^{(m)} \equiv |y_n^{(m)}\rangle\langle y_n^{(m)}|$ . These are related to the Ritz values as

$$\lambda_n^{(m)} = \langle y_n^{(m)} | T | y_n^{(m)} \rangle = \frac{\langle \psi | P_n^{(m)} T P_n^{(m)} | \psi \rangle}{|s_{1n}^{(m)}|^2 \langle \psi | \psi \rangle}. \quad (12)$$

For large  $m$ ,  $P_n^{(m)}$  converges to the projection operator  $|n\rangle\langle n|$  [46, 74]. A sufficiently good approximation  $P_n^{(m)} \approx |n\rangle\langle n|$  could remove contributions to the variance of  $\psi P_n^{(m)} T P_n^{(m)} \psi^\dagger$  from eigenstates with lower energy than  $2E_n$  in analogy to the variance reduction observed for  $\mathcal{O}(t)P\bar{\mathcal{O}}(0)$  correlation functions in Refs. [49–51]. It is possible that Lanczos provides such an approximation and prevents StN degradation once a certain level of projection accuracy is achieved. Since  $|n\rangle\langle n|$  projects to a particular eigenstate rather than just a global charge sector, this suggests that Lanczos results should also avoid exponential StN degradation for excited-state energies.

The ability of Lanczos algorithms to provide fast convergence and rigorous two-sided error bounds on LQCD energies while avoiding StN problems could be useful for a wide range of hadron spectroscopy calculations where isolating ground states is challenging including studies of nucleon, nuclear, and highly boosted systems.

## ACKNOWLEDGMENTS

I thank Dan Hackett, Benoît Assi, Zohreh Davoudi, Will Detmold, Dorota Grabowska, Anthony Grebe, Marc Illa, Will Jay, Andreas Kronfeld, Assumpta Parreño, Robert Perry, Martin Savage, Phiala Shanahan, and Ruth Van de Water for stimulating discussions and helpful comments. This manuscript has been authored by Fermi Research Alliance, LLC under Contract No. DE-AC02-07CH11359 with the U.S. Department of Energy, Office of Science, Office of High Energy Physics. This research used facilities of the USQCD Collaboration, which are funded by the Office of Science of the U.S. Department of Energy. The Chroma [83], QUDA [84–86], and QDP-JIT [87] software libraries were used in this work. Numerical analysis was performed and figures were produced using Mathematica [88].

- 
- [1] Y.-C. Jang, R. Gupta, B. Yoon, and T. Bhattacharya, Axial Vector Form Factors from Lattice QCD that Satisfy the PCAC Relation, *Phys. Rev. Lett.* **124**, 072002 (2020), arXiv:1905.06470 [hep-lat].
- [2] G. S. Bali, L. Barca, S. Collins, M. Gruber, M. Löffler, A. Schäfer, W. Söldner, P. Wein, S. Weishäupl, and T. Wurm (RQCD), Nucleon axial structure from lattice

- QCD, *JHEP* **05**, 126, arXiv:1911.13150 [hep-lat].
- [3] C. Alexandrou *et al.*, Nucleon axial and pseudoscalar form factors from lattice QCD at the physical point, *Phys. Rev. D* **103**, 034509 (2021), arXiv:2011.13342 [hep-lat].
- [4] S. Park, R. Gupta, B. Yoon, S. Mondal, T. Bhattacharya, Y.-C. Jang, B. Joó, and F. Winter (Nucleon Matrix Ele-

- ments (NME)), Precision nucleon charges and form factors using (2+1)-flavor lattice QCD, *Phys. Rev. D* **105**, 054505 (2022), arXiv:2103.05599 [hep-lat].
- [5] D. Djukanovic, G. von Hippel, J. Koponen, H. B. Meyer, K. Ottnad, T. Schulz, and H. Wittig, Isovector axial form factor of the nucleon from lattice QCD, *Phys. Rev. D* **106**, 074503 (2022), arXiv:2207.03440 [hep-lat].
- [6] Y.-C. Jang, R. Gupta, T. Bhattacharya, B. Yoon, and H.-W. Lin (Precision Neutron Decay Matrix Elements (PNDME)), Nucleon isovector axial form factors, *Phys. Rev. D* **109**, 014503 (2024), arXiv:2305.11330 [hep-lat].
- [7] C. Alexandrou, S. Bacchio, M. Constantinou, J. Finkenrath, R. Frezzotti, B. Kostrzewa, G. Koutsou, G. Spanoudes, and C. Urbach (Extended Twisted Mass), Nucleon axial and pseudoscalar form factors using twisted-mass fermion ensembles at the physical point, *Phys. Rev. D* **109**, 034503 (2024), arXiv:2309.05774 [hep-lat].
- [8] R. Gupta, Isovector Axial Charge and Form Factors of Nucleons from Lattice QCD, *PoS LATTICE2023*, 124 (2024).
- [9] A. Francis, J. R. Green, P. M. Junnarkar, C. Miao, T. D. Rae, and H. Wittig, Lattice QCD study of the  $H$  dibaryon using hexaquark and two-baryon interpolators, *Phys. Rev. D* **99**, 074505 (2019), arXiv:1805.03966 [hep-lat].
- [10] B. Hörz *et al.*, Two-nucleon S-wave interactions at the  $SU(3)$  flavor-symmetric point with  $m_{ud} \simeq m_s^{\text{phys}}$ : A first lattice QCD calculation with the stochastic Laplacian Heaviside method, *Phys. Rev. C* **103**, 014003 (2021), arXiv:2009.11825 [hep-lat].
- [11] S. Amarasinghe, R. Baghdadi, Z. Davoudi, W. Detmold, M. Illa, A. Parreño, A. V. Pochinsky, P. E. Shanahan, and M. L. Wagman, Variational study of two-nucleon systems with lattice QCD, *Phys. Rev. D* **107**, 094508 (2023), arXiv:2108.10835 [hep-lat].
- [12] J. R. Green, A. D. Hanlon, P. M. Junnarkar, and H. Wittig, Weakly bound  $H$  dibaryon from  $SU(3)$ -flavor-symmetric QCD, *Phys. Rev. Lett.* **127**, 242003 (2021), arXiv:2103.01054 [hep-lat].
- [13] W. Detmold, M. Illa, W. I. Jay, A. Parreño, R. J. Perry, P. E. Shanahan, and M. L. Wagman, Constraints on the finite volume two-nucleon spectrum at  $m_\pi \approx 806$  MeV, (2024), arXiv:2404.12039 [hep-lat].
- [14] G. Parisi, The Strategy for Computing the Hadronic Mass Spectrum, *Phys. Rept.* **103**, 203 (1984).
- [15] G. P. Lepage, The Analysis of Algorithms for Lattice Field Theory, in *Theoretical Advanced Study Institute in Elementary Particle Physics* (1989).
- [16] S. R. Beane, W. Detmold, T. C. Luu, K. Orginos, A. Parreño, M. J. Savage, A. Torok, and A. Walker-Loud (NPLQCD), High Statistics Analysis using Anisotropic Clover Lattices: (II) Three-Baryon Systems, *Phys. Rev. D* **80**, 074501 (2009), arXiv:0905.0466 [hep-lat].
- [17] S. R. Beane, W. Detmold, H.-W. Lin, T. C. Luu, K. Orginos, M. J. Savage, A. Torok, and A. Walker-Loud (NPLQCD), High Statistics Analysis using Anisotropic Clover Lattices: (III) Baryon-Baryon Interactions, *Phys. Rev. D* **81**, 054505 (2010), arXiv:0912.4243 [hep-lat].
- [18] Z. Davoudi, W. Detmold, K. Orginos, A. Parreño, M. J. Savage, P. Shanahan, and M. L. Wagman, Nuclear matrix elements from lattice QCD for electroweak and beyond-Standard-Model processes, *Phys. Rept.* **900**, 1 (2021), arXiv:2008.11160 [hep-lat].
- [19] G. Fox, R. Gupta, O. Martin, and S. Otto, Monte Carlo Estimates of the Mass Gap of the  $O(2)$  and  $O(3)$  Spin Models in (1+1)-dimensions, *Nucl. Phys. B* **205**, 188 (1982).
- [20] C. Michael and I. Teasdale, Extracting Glueball Masses From Lattice QCD, *Nucl. Phys. B* **215**, 433 (1983).
- [21] M. Lüscher and U. Wolff, How to Calculate the Elastic Scattering Matrix in Two-dimensional Quantum Field Theories by Numerical Simulation, *Nucl. Phys. B* **339**, 222 (1990).
- [22] B. Blossier, M. Della Morte, G. von Hippel, T. Mendes, and R. Sommer, On the generalized eigenvalue method for energies and matrix elements in lattice field theory, *JHEP* **04**, 094, arXiv:0902.1265 [hep-lat].
- [23] G. T. Fleming, Beyond Generalized Eigenvalues in Lattice Quantum Field Theory, in *40th International Symposium on Lattice Field Theory (2023)* arXiv:2309.05111 [hep-lat].
- [24] R. A. Briceño, J. J. Dudek, and R. D. Young, Scattering processes and resonances from lattice QCD, *Rev. Mod. Phys.* **90**, 025001 (2018), arXiv:1706.06223 [hep-lat].
- [25] J. Bulava *et al.*, Hadron Spectroscopy with Lattice QCD, in *Snowmass 2021* (2022) arXiv:2203.03230 [hep-lat].
- [26] A. D. Hanlon, Hadron spectroscopy and few-body dynamics from Lattice QCD, *PoS LATTICE2023*, 106 (2024), arXiv:2402.05185 [hep-lat].
- [27] G. T. Fleming, What can lattice QCD theorists learn from NMR spectroscopists?, in *3rd International Workshop on Numerical Analysis and Lattice QCD* (2004) pp. 143–152, arXiv:hep-lat/0403023.
- [28] S. R. Beane, W. Detmold, T. C. Luu, K. Orginos, A. Parreno, M. J. Savage, A. Torok, and A. Walker-Loud, High Statistics Analysis using Anisotropic Clover Lattices: (I) Single Hadron Correlation Functions, *Phys. Rev. D* **79**, 114502 (2009), arXiv:0903.2990 [hep-lat].
- [29] M. Fischer, B. Kostrzewa, J. Ostmeier, K. Ottnad, M. Ueding, and C. Urbach, On the generalised eigenvalue method and its relation to Prony and generalised pencil of function methods, *Eur. Phys. J. A* **56**, 206 (2020), arXiv:2004.10472 [hep-lat].
- [30] C. Lanczos, An iteration method for the solution of the eigenvalue problem of linear differential and integral operators, *J. Res. Natl. Bur. Stand. B* **45**, 255 (1950).
- [31] G. H. Golub and D. P. O’Leary, Some history of the conjugate gradient and Lanczos algorithms: 1948–1976, *SIAM Review* **31**, 50 (1989), <https://doi.org/10.1137/1031003>.
- [32] B. N. Parlett, Do we fully understand the symmetric Lanczos algorithm yet (1995).
- [33] G. Meurant and Z. Strakoš, The Lanczos and conjugate gradient algorithms in finite precision arithmetic, *Acta Numerica* **15**, 471 (2006).
- [34] Y. Saad, *Numerical Methods for Large Eigenvalue Problems: Revised Edition*, Classics in Applied Mathematics (Society for Industrial and Applied Mathematics, 2011).
- [35] G. H. Golub and C. F. Van Loan, *Matrix Computations* (Johns Hopkins University Press, Philadelphia, PA, 2013).
- [36] V. Hernandez, J. E. Roman, A. Tomas, and V. Vidal, *A survey of software for sparse eigenvalue problems*, Tech. Rep. STR-5 (Universitat Politècnica de València, 2006) available at <https://slepc.upv.es>.
- [37] M. Caffarel, F. X. Gadea, and D. M. Ceperley, Lanczós-type algorithm for quantum monte carlo data, Euro-

- physics Letters **16**, 249 (1991).
- [38] S. Sorella, Generalized Lanczos algorithm for variational quantum monte carlo, *Physical Review B* **64**, 10.1103/physrevb.64.024512 (2001).
- [39] F. Becca and S. Sorella, *Quantum Monte Carlo Approaches for Correlated Systems* (Cambridge University Press, 2017).
- [40] T. Kalkreuter, Study of Cullum’s and Willoughby’s Lanczos method for Wilson fermions, *Comput. Phys. Commun.* **95**, 1 (1996), arXiv:hep-lat/9509071.
- [41] A. D. Kennedy, I. Horvath, and S. Sint, A New exact method for dynamical fermion computations with nonlocal actions, *Nucl. Phys. B Proc. Suppl.* **73**, 834 (1999), arXiv:hep-lat/9809092.
- [42] M. A. Clark, C. Jung, and C. Lehner, Multi-Grid Lanczos, *EPJ Web Conf.* **175**, 14023 (2018), arXiv:1710.06884 [hep-lat].
- [43] H. Jeong, C. DeTar, and S. Gottlieb, Performance of several Lanczos eigensolvers with HISQ fermions, *PoS LATTICE2021*, 053 (2022), arXiv:2201.03755 [hep-lat].
- [44] S. Kaniel, Estimates for some computational techniques in linear algebra, *Mathematics of Computation* **20**, 369 (1966).
- [45] C. C. Paige, *The Computation of Eigenvalues and Eigenvectors of Very Large Sparse Matrices*, Ph.D. thesis, London University, London, UK (1971).
- [46] Y. Saad, On the rates of convergence of the Lanczos and the block-Lanczos methods, *SIAM Journal on Numerical Analysis* **17**, 687 (1980).
- [47] J. Garza-Vargas and A. Kulkarni, The Lanczos algorithm under few iterations: Concentration and location of the output, *SIAM Journal on Matrix Analysis and Applications* **41**, 1312–1346 (2020).
- [48] J. B. Kogut and L. Susskind, Hamiltonian Formulation of Wilson’s Lattice Gauge Theories, *Phys. Rev. D* **11**, 395 (1975).
- [49] M. Della Morte and L. Giusti, Exploiting symmetries for exponential error reduction in path integral Monte Carlo, *Comput. Phys. Commun.* **180**, 813 (2009).
- [50] M. Della Morte and L. Giusti, Symmetries and exponential error reduction in Yang-Mills theories on the lattice, *Comput. Phys. Commun.* **180**, 819 (2009), arXiv:0806.2601 [hep-lat].
- [51] M. Della Morte and L. Giusti, A novel approach for computing glueball masses and matrix elements in Yang-Mills theories on the lattice, *JHEP* **05**, 056, arXiv:1012.2562 [hep-lat].
- [52] M. Lüscher, Construction of a Selfadjoint, Strictly Positive Transfer Matrix for Euclidean Lattice Gauge Theories, *Commun. Math. Phys.* **54**, 283 (1977).
- [53] M. Lüscher and P. Weisz, Definition and General Properties of the Transfer Matrix in Continuum Limit Improved Lattice Gauge Theories, *Nucl. Phys. B* **240**, 349 (1984).
- [54] R. V. Mises and H. Pollaczek-Geiringer, Praktische Verfahren der Gleichungsaufösung, *Zeitschrift Angewandte Mathematik und Mechanik* **9**, 58 (1929).
- [55] B. N. Parlett, H. Simon, and L. M. Stringer, On estimating the largest eigenvalue with the Lanczos algorithm, *Mathematics of Computation* **38**, 153 (1982).
- [56] J. Kuczyński and H. Woźniakowski, Estimating the largest eigenvalues by the power and Lanczos algorithms with a random start, *SIAM J. Matrix Anal. Appl.* **13**, 1094–1122 (1992).
- [57] B. Parlett, Misconvergence in the Lanczos algorithm, in *Reliable Numerical Computation* (Oxford University Press, 1990) <https://academic.oup.com/book/0/chapter/422058476/chapter-pdf/52393581/isbn-9780198535645-book-part-2.pdf>.
- [58] A. B. J. Kuijlaars, Which eigenvalues are found by the Lanczos method?, *SIAM Journal on Matrix Analysis and Applications* **22**, 306 (2000), <https://doi.org/10.1137/S089547989935527X>.
- [59] W. DeMeo, *A Lanczos Procedure for Approximating Eigenvalues of Large Stochastic Matrices*, Ph.D. thesis (1998).
- [60] J. H. J. H. Wilkinson, *The algebraic eigenvalue problem*, Monographs on numerical analysis (Clarendon Press, Oxford, 1965).
- [61] B. N. Parlett and D. S. Scott, The Lanczos algorithm with selective orthogonalization, *Mathematics of Computation* **33**, 217 (1979).
- [62] J. J. Dudek, R. G. Edwards, and C. E. Thomas (Hadron Spectrum), Energy dependence of the  $\rho$  resonance in  $\pi\pi$  elastic scattering from lattice QCD, *Phys. Rev. D* **87**, 034505 (2013), [Erratum: *Phys.Rev.D* 90, 099902 (2014)], arXiv:1212.0830 [hep-ph].
- [63] C. B. Lang and V. Verduci, Scattering in the  $\pi N$  negative parity channel in lattice QCD, *Phys. Rev. D* **87**, 054502 (2013), arXiv:1212.5055 [hep-lat].
- [64] D. J. Wilson, R. A. Brice no, J. J. Dudek, R. G. Edwards, and C. E. Thomas, Coupled  $\pi\pi$ ,  $K\bar{K}$  scattering in  $P$ -wave and the  $\rho$  resonance from lattice QCD, *Phys. Rev. D* **92**, 094502 (2015), arXiv:1507.02599 [hep-ph].
- [65] J. Cullum and R. A. Willoughby, Computing eigenvalues of very large symmetric matrices—an implementation of a Lanczos algorithm with no reorthogonalization, *Journal of Computational Physics* **44**, 329 (1981).
- [66] J. K. Cullum and R. A. Willoughby, *Lanczos procedures, in Lanczos Algorithms for Large Symmetric Eigenvalue Computations Vol. I Theory* (Birkhäuser Boston, Boston, MA, 1985) pp. 92–163.
- [67] B. N. Parlett, D. R. Taylor, and Z. A. Liu, A look-ahead Lanczos algorithm for unsymmetric matrices, *Mathematics of Computation* **44**, 105 (1985).
- [68] N. M. Nachtigal, *A look-ahead variant of the Lanczos algorithm and its application to the quasi-minimal residual method for non-Hermitian linear systems*, Ph.D. thesis (1993).
- [69] U. Elsner, V. Mehrmann, F. Milde, R. A. Römer, and M. Schreiber, The Anderson model of localization: A challenge for modern eigenvalue methods, *SIAM Journal on Scientific Computing* **20**, 2089–2102 (1999).
- [70] B. Efron, *The Jackknife, the bootstrap and other resampling plans*, Regional Conference Series in applied mathematics No. 38 (Society for Industrial and Applied Mathematics, Philadelphia, Pa., 1982).
- [71] A. C. Davison and D. V. Hinkley, The basic bootstraps, in *Bootstrap Methods and their Application*, Cambridge Series in Statistical and Probabilistic Mathematics (Cambridge University Press, 1997) p. 11–69.
- [72] P. Young, Everything you wanted to know about data analysis and fitting but were afraid to ask (2014), arXiv:1210.3781 [physics.data-an].
- [73] P. Lepage, C. Gohlke, and D. Hackett, `gplepage/gvar`: `gvar` version 13.1 (2024).
- [74] Y. Saad, The Lanczos biorthogonalization algorithm and other oblique projection methods for solving large unsymmetric systems, *SIAM Journal on Numerical Analy-*

- sis **19**, 485 (1982), <https://doi.org/10.1137/0719031>.
- [75] M. L. Wagman and M. J. Savage, Statistics of baryon correlation functions in lattice QCD, *Phys. Rev. D* **96**, 114508 (2017), [arXiv:1611.07643](https://arxiv.org/abs/1611.07643) [hep-lat].
- [76] W. Detmold, G. Kanwar, and M. L. Wagman, Phase Unwrapping and One-Dimensional Sign Problems, *Phys. Rev. D* **98**, 074511 (2018), [arXiv:1806.01832](https://arxiv.org/abs/1806.01832) [hep-lat].
- [77] S. R. Beane *et al.* (NPLQCD, QCDSF), Charged multihadron systems in lattice QCD+QED, *Phys. Rev. D* **103**, 054504 (2021), [arXiv:2003.12130](https://arxiv.org/abs/2003.12130) [hep-lat].
- [78] B. Yoon *et al.*, Isovector charges of the nucleon from 2+1-flavor QCD with clover fermions, *Phys. Rev. D* **95**, 074508 (2017), [arXiv:1611.07452](https://arxiv.org/abs/1611.07452) [hep-lat].
- [79] S. Mondal, R. Gupta, S. Park, B. Yoon, T. Bhattacharya, B. Joó, and F. Winter (Nucleon Matrix Elements (NME)), Nucleon momentum fraction, helicity and transversity from 2+1-flavor lattice QCD, *JHEP* **21**, 004, [arXiv:2011.12787](https://arxiv.org/abs/2011.12787) [hep-lat].
- [80] M. Lüscher and P. Weisz, On-shell improved lattice gauge theories, *Commun. Math. Phys.* **98**, 433 (1985), [Erratum: *Commun.Math.Phys.* 98, 433 (1985)].
- [81] B. Sheikholeslami and R. Wohlert, Improved Continuum Limit Lattice Action for QCD with Wilson Fermions, *Nucl. Phys. B* **259**, 572 (1985).
- [82] C. Morningstar and M. J. Peardon, Analytic smearing of SU(3) link variables in lattice QCD, *Phys. Rev. D* **69**, 054501 (2004), [arXiv:hep-lat/0311018](https://arxiv.org/abs/hep-lat/0311018).
- [83] R. G. Edwards and B. Joó (SciDAC, LHPC, UKQCD), The Chroma software system for lattice QCD, *Nucl. Phys. B Proc. Suppl.* **140**, 832 (2005), [arXiv:hep-lat/0409003](https://arxiv.org/abs/hep-lat/0409003).
- [84] M. A. Clark, R. Babich, K. Barros, R. C. Brower, and C. Rebbi (QUDA), Solving Lattice QCD systems of equations using mixed precision solvers on GPUs, *Comput. Phys. Commun.* **181**, 1517 (2010), [arXiv:0911.3191](https://arxiv.org/abs/0911.3191) [hep-lat].
- [85] R. Babich, M. A. Clark, B. Joó, G. Shi, R. C. Brower, and S. Gottlieb (QUDA), Scaling lattice QCD beyond 100 GPUs, in *International Conference for High Performance Computing, Networking, Storage and Analysis* (2011) [arXiv:1109.2935](https://arxiv.org/abs/1109.2935) [hep-lat].
- [86] M. A. Clark, B. Joó, A. Strelchenko, M. Cheng, A. Gambhir, and R. C. Brower (QUDA), Accelerating lattice QCD multigrid on GPUs using fine-grained parallelization, in *International Conference for High Performance Computing, Networking, Storage and Analysis* (2016) [arXiv:1612.07873](https://arxiv.org/abs/1612.07873) [hep-lat].
- [87] F. Winter, M. Clark, R. Edwards, and B. Joó, A framework for lattice qcd calculations on gpus, in *2014 IEEE 28th International Parallel and Distributed Processing Symposium* (2014) pp. 1073–1082.
- [88] Wolfram Research Inc., Mathematica, Version 14.0, <https://www.wolfram.com/mathematica>.
- [89] J. Wilkinson, Global convergence of tridiagonal QR algorithm with origin shifts, *Linear Algebra and its Applications* **1**, 409 (1968).
- [90] T.-L. Wang and W. B. Gragg, Convergence of the shifted qr algorithm for unitary hessenberg matrices, *Mathematics of Computation* **71**, 1473 (2002).
- [91] D. C. Hackett, P. R. Oare, D. A. Pefkou, and P. E. Shanahan, Gravitational form factors of the pion from lattice QCD, *Phys. Rev. D* **108**, 114504 (2023), [arXiv:2307.11707](https://arxiv.org/abs/2307.11707) [hep-lat].
- [92] R. Abbott, W. Detmold, M. Illa, A. Parreño, R. J. Perry, F. Romero-López, P. E. Shanahan, and M. L. Wagman, QCD constraints on isospin-dense matter and the nuclear equation of state, (2024), [arXiv:2406.09273](https://arxiv.org/abs/2406.09273) [hep-lat].

## SUPPLEMENTARY MATERIAL

This Supplementary Material provides additional details on the implementation of the Lanczos algorithm used to compute the results of the main text. A proof that thermal effects can be described without modifying the basic algorithm is presented in Sec. A. Recursion relations for symmetric Lanczos are presented in Sec. B. An implementation of the Cullum-Willoughby method for removing spurious eigenvalues is introduced and its numerical application described in Sec. C. An oblique Lanczos method suitable for describing noisy Monte Carlo results leading to non-Hermitian  $T_{ij}^{(m)}$  is presented in Sec. D. Finally, Sec. E presents additional numerical results on the residuals and correlations of Lanczos results.

### A. Thermal effects

Consider a function  $f(t)$  sampled at discrete points  $t \in \{a, 2a, \dots, \beta a\}$  with a spectral representation

$$f(t) = \sum_{n=0}^{\infty} X_n e^{-E_n t} + Y_n e^{F_n t}, \quad (13)$$

where  $E_n, F_n > 0$  and  $X_n, Y_n \in \mathbb{R}$ . Particular cases include bosonic thermal correlation functions in which  $Y_n = X_n e^{-\beta E_n}$  and  $F_n = E_n$ , as well as fermionic thermal correlation functions in which the  $F_n$  are equal to energies of fermionic states with opposite parity to those with energies  $E_n$  and the  $Y_n$  have opposite signs to the  $X_n$ . The thermal states with transfer matrix eigenvalues  $e^{aF_n}$  can be treated as additional states on equal footing with those with eigenvalues  $e^{-aE_n}$  by defining

$$f(t) = \sum_{k=0}^{\infty} Z_k e^{L_k t}, \quad (14)$$

where

$$Z_k \equiv \begin{cases} X_{k/2}, & k \text{ even} \\ Y_{(k-1)/2}, & k \text{ odd} \end{cases}, \quad (15)$$

$$L_k \equiv \begin{cases} -E_{k/2}, & k \text{ even} \\ F_{(k-1)/2}, & k \text{ odd} \end{cases}.$$

Using this representation as a starting point, a matrix  $T$  can be defined that acts analogously to the physical transfer matrix in the zero-temperature case.

A set of vectors  $|k\rangle$  and dual vectors  $\langle k|$  can be defined to have inner product  $\langle k|k'\rangle = \delta_{kk'}$ . A vector  $|\psi\rangle$  can be defined by

$$\langle k|\psi\rangle \equiv \sqrt{Z_k}, \quad (16)$$

where the branch cut of  $\sqrt{Z_k}$  is placed along the negative imaginary axis in case  $Z_k$  is negative. The dual vector  $\langle \chi|$  can be defined by

$$\langle \chi|k\rangle \equiv \sqrt{Z_k}, \quad (17)$$

An operator  $T$  can be defined by

$$\langle k|T|k'\rangle = e^{aL_k} \delta_{kk'}. \quad (18)$$

Since  $L_k \in \mathbb{R}$ ,  $T$  is represented by a real and diagonal matrix in the  $|k\rangle$  basis and is therefore a Hermitian operator. This provides a matrix-element representation for  $f(t)$  as

$$\begin{aligned} \langle \chi|T^{t/a}|\psi\rangle &= \sum_{k,k'} \langle \chi|k\rangle \langle k|T^{t/a}|k'\rangle \langle k'|\psi\rangle \\ &= \sum_{k,k'} \sqrt{Z_k} e^{L_k t} \delta_{kk'} \sqrt{Z_{k'}} \\ &= \sum_k Z_k e^{L_k t} \\ &= f(t). \end{aligned} \quad (19)$$

Regardless of whether  $f(t)$  can be associated with a physical correlation function, this provides a representation of  $f(a), f(2a), \dots, f(t)$  as matrix elements  $\langle \chi|T|\psi\rangle, \langle \chi|T^2|\psi\rangle, \dots, \langle \chi|T^{t/a}|\psi\rangle$  of a Hermitian operator  $T$ . Application of the Lanczos algorithm described here to  $f(t)$  will lead to iterative approximations  $\lambda_k^{(m)}$  that converge to eigenvalues  $e^{aL_k}$  of  $T$  in the limit of large Lanczos steps  $m \rightarrow \infty$ . This implies

$$\{\lambda_k^{(m)}\} \rightarrow \{e^{aL_k}\} = \{e^{-aE_n}, e^{aF_n}\}, \quad (20)$$

and the estimators  $E_k^{(m)} = -(1/a) \ln \lambda_k^{(m)}$  therefore converge to

$$\{E_k^{(m)}\} \rightarrow \{E_n, -F_n\}. \quad (21)$$

The “energy spectrum” obtained by applying Lanczos methods to  $f(t)$  for  $m$  steps will therefore approximate some admixture of the  $E_n$  and  $-F_n$ .

Applying Lanczos methods to bosonic thermal correlation functions will therefore result in positive  $E_n^{(m)}$  approximating physical energies  $E_n$  and negative  $E_n^{(m)}$  approximating  $-E_n$ . Applying Lanczos methods to fermionic thermal correlation functions will result in positive  $E_n^{(m)}$  approximating the energies of fermionic states with the same parity as  $|\psi\rangle$  and negative  $E_n^{(m)}$  approximating minus the energies of states with opposite parity.

Since this construction applies even when some of the  $X_n$  are negative, it is valid even when  $f(t)$  describes an “asymmetric” correlation function represented as  $\langle \mathcal{O}'(t)\mathcal{O}^\dagger(0)\rangle$  with  $\mathcal{O} \neq \mathcal{O}'$  in the physical Hilbert space. An oblique Lanczos method suitable for asymmetric correlation functions is described in Sec. D below.

The practical convergence of Lanczos-based estimators for time series of the form Eq. (13) that can be interpreted as bosonic and fermionic thermal correlation functions with  $\beta/a = 100$  are shown in Figs. 4-5. Thermal states show up as negative-energy eigenvalues in Lanczos results for  $t/a \gtrsim 20$ . In the same region, the approach of the Lanczos estimator to the ground-state energy is

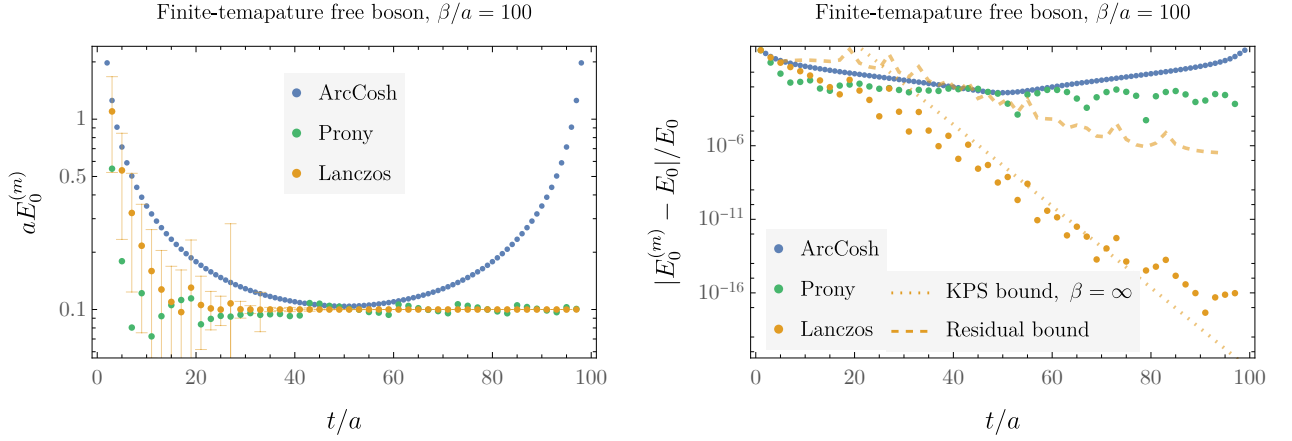


FIG. 4. Comparison of the estimator  $\text{arccosh}[(C(t+2a) + C(t))/(2C(t+a))]$  with Prony- and Lanczos-based estimators for a time series with  $\beta/a = 100$  points corresponding to Eq. (13) with  $X_n = Y_n = (n+1)$  and  $aE_n = 0.1(n+1)$  for  $n = 0, \dots, 50$ . As in Fig. 1, estimators  $E_0^{(k)}$  after  $k$  iterations of Lanczos and/or Prony are shown at  $t/a = 2k - 1$  since this is the largest  $t/a$  correlation function involved in its calculation. The residual bound computed via the Lanczos algorithm with Eq. (9) is shown as a dashed line. The ground-state version of the KPS bound, Eq. (7), only applies for  $\beta \rightarrow \infty$  limit and can be violated when thermal effects in  $f(t)$  are significant.

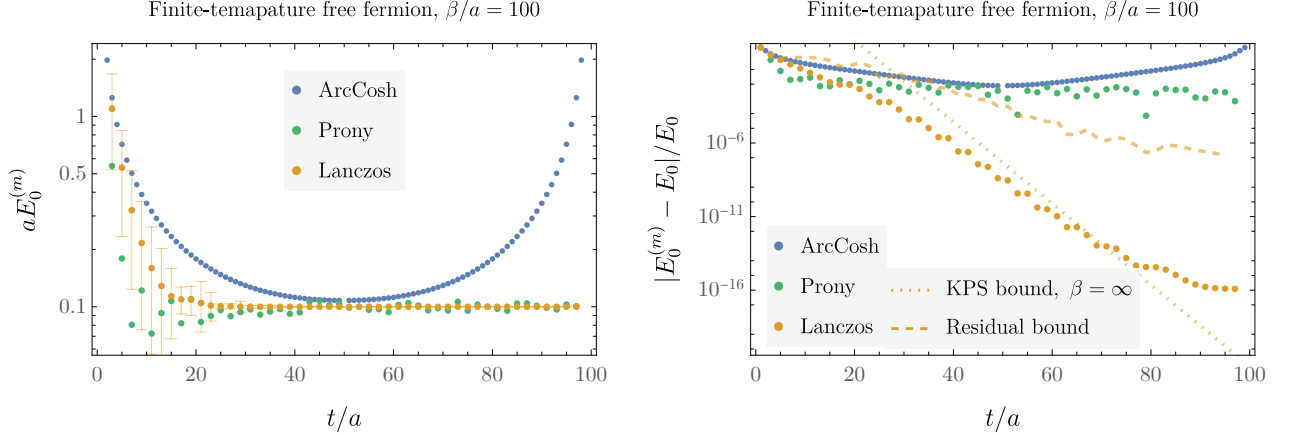


FIG. 5. Thermal fermion results analogous to Eq. (4).

non-monotonic. The residual bound applies for all  $t/a$  and provides a rigorous systematic uncertainty on the distance between  $E^{(k)}$  and some energy eigenvalue. The ground-state version of the KPS bound in the form of Eq. (7) only applies for  $\beta \rightarrow \infty$  — empirically it holds for  $t \lesssim 3/4\beta$  in this example but can be seen to be violated for larger  $t$ .

A bound valid at finite  $\beta$  can be obtained from the general form of the KPS bound [44–46],

$$0 \leq \lambda_n^{(m)} - \lambda_n \leq (\lambda_n - \lambda_\infty) \left[ \frac{K_n^{(m)} \tan \phi_n}{T_{m-n}(\Gamma_n)} \right]^2, \quad (22)$$

where the smallest eigenvalue of the transfer matrix is denoted  $\lambda_\infty$  and converges to zero for a lattice gauge theory with an infinite-dimensional Hilbert space such as

LQCD,  $\cos \phi_n \equiv \langle n | \psi \rangle = Z_n$ ,

$$\Gamma_n \equiv 1 + \frac{2(\lambda_n - \lambda_{n+1})}{\lambda_{n+1} - \lambda_\infty} = 2e^{a(E_{n+1} - E_n)} - 1, \quad (23)$$

and

$$K_n^{(m)} \equiv \prod_{l=1}^{n-1} \frac{\lambda_l^{(m)} - \lambda_\infty}{\lambda_l^{(m)} - \lambda_l}, \quad n > 0, \quad (24)$$

with  $K_0^{(m)} \equiv 1$ . However, this bound requires knowledge of the entire spectrum to compute. Only for the case of  $n = 0$  does the bound reduce to an expression in terms of only  $E_n$  and  $Z_n$ , which results in Eq. (7).

## B. Recursion relations

A recursive application of Lanczos suitable for infinite-dimensional transfer matrices involves the scalar matrix elements  $F_j^k = \langle v_j | T^k | v_j \rangle$  and  $G_j^k = \langle v_j | T^k | v_{j-1} \rangle$ . The recursion base case is

$$F_1^k = \langle v_1 | T^k | v_1 \rangle = \frac{\langle \psi | T^k | \psi \rangle}{\langle \psi | \psi \rangle} = \frac{C(ka)}{C(0)}, \quad (25)$$

$$G_1^k = 0.$$

The tridiagonal matrix elements  $\alpha_1$  and  $\beta_2$  can then be obtained using the general relations

$$\alpha_j = F_j^1, \quad (26)$$

$$\beta_{j+1} = \sqrt{F_j^2 - \alpha_j^2 - \beta_j^2},$$

where  $\beta_1 = 0$  by assumption.

The three-term recurrence in Eq. (6) can be substituted in to the definitions of  $F_j^k = \langle v_j | T^k | v_j \rangle$  and  $G_j^k = \langle v_j | T^k | v_{j-1} \rangle$  to derive recursion relations directly for these matrix elements as

$$F_{j+1}^k = \frac{1}{\beta_{j+1}^2} [F_j^{k+2} + \alpha_j^2 F_j^k + \beta_j^2 F_{j-1}^k - 2\alpha_j F_j^{k+1} + 2\alpha_j \beta_j G_j^k - 2\beta_j G_j^{k+1}], \quad (27)$$

and

$$G_{j+1}^k = \frac{1}{\beta_{j+1}} [F_j^{k+1} - \alpha_j F_j^k - \beta_j G_j^k], \quad (28)$$

for  $k \in \{1, \dots, m - 2(j - 1)\}$ . After computing the  $\alpha_j$  and  $\beta_j$  for  $j \in \{1, \dots, m\}$ , the tridiagonal matrix  $T_{ij}^{(m)}$  can be constructed as,

$$T_{ij}^{(m)} = \begin{pmatrix} \alpha_1 & \beta_2 & & & & & 0 \\ \beta_2 & \alpha_2 & \beta_3 & & & & \\ & \beta_3 & \alpha_3 & \ddots & & & \\ & & \ddots & \ddots & \beta_{m-1} & & \\ 0 & & & \beta_{m-1} & \alpha_{m-1} & \beta_m & \\ & & & & \beta_m & \alpha_m & \end{pmatrix}_{ij}, \quad (29)$$

and its eigenvalues  $\lambda_k^{(m)}$  and eigenvectors  $s_k^{(m)}$  computed efficiently [89, 90]. A Lanczos estimate of the  $k$ -th energy is then given by

$$E_k^{(m)} = -\frac{1}{a} \ln \lambda_k^{(m)}. \quad (30)$$

With  $m = 1$ , the only element of  $T_{ij}^{(m)}$  is  $T_{11}^{(1)} = \alpha_1$ , which corresponds to

$$\alpha_1 = F_1^1 = \frac{C(a)}{C(0)} \equiv \hat{C}(a), \quad (31)$$

The Lanczos estimator with  $m = 1$  is therefore equivalent to the effective mass,  $E_0^{(1)} = E(a)$ . The next iteration involves  $\beta_2 = \sqrt{\hat{C}(2a) - \hat{C}(a)^2}$  and

$$\alpha_2 = \frac{\hat{C}(3a) - 2\hat{C}(2a)\hat{C}(a) + \hat{C}(a)^3}{\hat{C}(2a) - \hat{C}(a)^2}, \quad (32)$$

which are real and positive by the assumption of Hermiticity of  $T$  and therefore convexity of  $\hat{C}(t)$ . The eigenvalues of  $T_{ij}^{(2)}$  are given in terms of these as

$$\lambda_{0/1}^{(2)} = \frac{1}{2} \left[ \alpha_1 + \alpha_2 \pm \sqrt{4\beta_2^2 + (\alpha_1 - \alpha_2)^2} \right]. \quad (33)$$

In general  $\alpha_j$  is a rational function of  $\hat{C}(a), \dots, \hat{C}(2ja)$ ,  $\beta_j^2$  is a rational function of  $\hat{C}(a), \dots, \hat{C}(2(j-1)a)$ , and the  $\lambda_j^{(m)}$  are the roots of the characteristic polynomial of a  $2j \times 2j$  matrix involving  $\hat{C}(a), \dots, \hat{C}(2ja)$ .

## C. Spurious eigenvalues

Implementing the Cullum-Willoughby procedure [65, 66] for removing spurious eigenvalues in Lanczos applications to noisy Monte Carlo results requires the definition of a threshold for when eigenvalues of  $T_{ij}^{(m)}$  and  $\tilde{T}_{ij}^{(m)}$  should be considered identical, where  $\tilde{T}_{ij}^{(m)}$  is the matrix obtained by removing the first row and column from the tridiagonal matrix  $T_{ij}^{(m)}$ . The threshold should only be different from zero because of statistical uncertainties (and to a lesser extent finite-precision arithmetic used when generating field configurations and/or executing the Lanczos algorithm). An automated procedure for choosing this threshold based on bootstrap eigenvalue histograms is defined below. It introduces two hyperparameters:  $\Delta$  controls the number of histogram bins and  $K_{CW}$  is an  $\mathcal{O}(1)$  tolerance parameter specifying how many samples are required to call a bin “non-spurious” as described below.

Since  $T$  has only positive eigenvalues by assumption, non-positive eigenvalues of  $T_{ij}^{(m)}$  must be spurious eigenvalues arising from statistical noise. Using the oblique Lanczos formalism described in Sec. D below, the  $T_{ij}^{(m)}$  are all real and the Ritz values  $\lambda_k^{(m)}$  are therefore either exactly real or have non-zero imaginary parts and come in complex conjugate pairs.<sup>2</sup> All Ritz values that have non-zero imaginary parts at working precision can therefore be discarded as spurious (in the numerical examples here

<sup>2</sup> Using the symmetric Lanczos algorithm with complex  $\beta_j$  introduces small but non-zero imaginary parts to all eigenvalues and a threshold for distinguishing positive from non-positive eigenvalues must be introduced.

I discard Ritz values with  $|\arg(\lambda_k^{(m)})| > 10^{-12}$ . Using arbitrary-precision arithmetic instead of double precision leads to significant changes to complex Ritz values but provides consistent results for positive Ritz values, and in the Monte Carlo analyses here I have adopted double precision for convenience.<sup>3</sup>

Bootstrap resampling [70–72] can help to identify spurious eigenvalues because they arise due to statistical noise and their values are therefore more sensitive to noise than non-spurious eigenvalues. Ritz values are computed for sample mean correlation functions and for each of  $N_{\text{boot}}$  ensembles obtained using bootstrap resampling [70–72]. In the numerical results of this work,  $N_{\text{boot}} = 200$  is used throughout.

The bootstrap Ritz value distribution can be analyzed using a variation of the Cullum-Willoughby criterion:

- Compute the Ritz values  $\lambda_k^{(b,m)}$  with  $k \in \{1, \dots, m\}$  an arbitrary ordering,  $m \in \{1, \dots, N_{\text{it}}\}$  where  $N_{\text{it}} = (\beta + 1)/2$  is the maximum number of Lanczos iterations, and  $b \in \{1, \dots, N_{\text{boot}}\}$ .
- Discard any  $\lambda_k^{(b,m)}$  with non-zero imaginary parts as spurious.
- Compute the eigenvalues  $\tau_k^{(b,m)}$  of the matrices  $\tilde{T}_{ij}^{(b,m)}$  obtained by removing the first row and column of  $T_{ij}^{(b,m)}$  for each  $m$  and  $b$ .
- Compute  $d_k^{(b,m)} \equiv \min_{j \in \{1, \dots, m-1\}} |\lambda_k^{(b,m)} - \tau_j^{(b,m)}|$  for all  $k$ ,  $m$ , and  $b$ .
- Denote the total number of approximately positive eigenvalues computed across all bootstrap ensembles by  $N_+$ . Define the number of eigenvalues that could be determined if these were all non-spurious by  $N_\lambda \equiv \text{round}[N_+/N_{\text{boot}}/N_{\text{it}}]$  where round denotes rounding to the nearest integer.
- Histogram  $\ln d_k^{(b,m)}$  with a number of bins defined by  $N_{\text{bins}} \equiv \Delta N_\lambda$ . The appropriate value of the  $\mathcal{O}(1)$  hyperparameter  $\Delta$  depends on the working precision since the  $d_k^{(b,m)}$  can get very small using arbitrary-precision arithmetic; using double precision the energy results and uncertainties studied here are insensitive to  $\Delta$  over the range  $\Delta \sim 2 - 10$ . For concreteness I take  $\Delta = 4$  everywhere.
- Define  $\delta_{CW} \equiv N_{\text{boot}}(N_{\text{it}} - N_\lambda)K_{CW}/\Delta$ , the number of counts required to indicate a bin contains an eigenvalue that is repeated across Lanczos iterations and bootstrap ensembles and is therefore not spurious. Here,  $K_{CW}$  is a  $\mathcal{O}(1)$  hyperparameter discussed more below; I take  $K_{CW} = 3$  everywhere.

- Find the first histogram bin (ordered with  $\ln d_k^{(b,m)}$  increasing) with more than  $\delta_{CW}$  counts. Denoting this histogram bin by  $\ln d_k^{(b,m)} \in [B_i, B_{i+1}]$ , define the Cullum-Willoughby threshold by  $\varepsilon_{CW} \equiv e^{B_{i-1}}$ .

The result of this bootstrap histogram analysis is the Cullum-Willoughby threshold  $\varepsilon_{CW}$ . This threshold is used to remove spurious Ritz values:

- Compute the sample mean Ritz values,  $\lambda_k^{(m)}$ , and discard  $\lambda_k^{(m)}$  with non-zero imaginary parts. Compute the eigenvalues  $\tau_k^{(m)}$  and distances  $d_k^{(m)}$ . Remove  $\lambda_k^{(m)}$  with  $d_k^{(m)} > \varepsilon_{CW}$  as spurious.
- Remove Ritz values with  $\lambda_k^{(m)} > 1$ , which correspond to thermal states as described in Sec. A.
- The remaining non-spurious Ritz values  $\lambda_k^{(m)} < 1$  are sorted as  $\lambda_0^{(m)} > \lambda_1^{(m)} > \dots$  for each  $m$ .

These provide Lanczos energies  $E_k^{(m)} \equiv -(1/a) \ln \lambda_k^{(m)}$  and in particular the central values for  $E_0^{(m)}$  used here.

Bootstrap samples in which the ground-state energy eigenvalue is misidentified as either an excited-state energy eigenvalue or as a spurious Ritz value can and do occur in practice. Some form of robust estimator must therefore be employed to prevent uncertainty estimates from being artificially inflated by outliers. Here, I adopt the following procedure

- Define  $\lambda_0^{(b,m)}$  with  $b \in \{1, \dots, N_{\text{boot}}\}$  to be the positive Ritz value closest to  $\lambda_0^{(m)}$  for each  $b$ . Define  $s_0^{(b,m)}$  to be the corresponding eigenvector.
- Define  $E_0^{(b,m)} \equiv -\ln \lambda_0^{(b,m)}$  and symmetric Lanczos residuals  $R_0^{(b,m)} \equiv (\beta_{m+1}^{(b)})^2 |s_{m0}^{(b,m)}|^2$ . For oblique Lanczos define  $R_0^{(b,m)}$  to be the minimum of Eq. (74) and Eq. (79) computed for each bootstrap ensemble.
- Define  $\delta E_0^{(m)}$  as the  $1\sigma$  bootstrap empirical confidence interval [70–72] of the  $E_0^{(b,m)}$ . Similarly define  $\delta R_0^{(m)}$  as the  $1\sigma$  bootstrap empirical confidence interval of the  $R_0^{(b,m)}$ .
- Define the central value of  $R_0^{(m)}$  to be the median of the  $R_0^{(b,m)}$ .

The same procedure can be applied to excited-state Ritz values. This use of bootstrap confidence intervals and median estimators (for  $R_0^{(m)}$  in this case) is a procedure used in LQCD data analyses [73]. In the examples studied here, I find that bootstrap results for  $E_0^{(b,m)}$  are occasionally very close to  $E_1^{(m)}$  rather than  $E_0^{(m)}$  and there are apparent outliers in  $R_0^{(b,m)}$ . It is likely that the introduction of more sophisticated robust estimators can

<sup>3</sup> It is likely that calculations employing significantly larger imaginary time extents and Lanczos iteration counts than those studied here would need to employ higher precision during execution of the Lanczos algorithm.

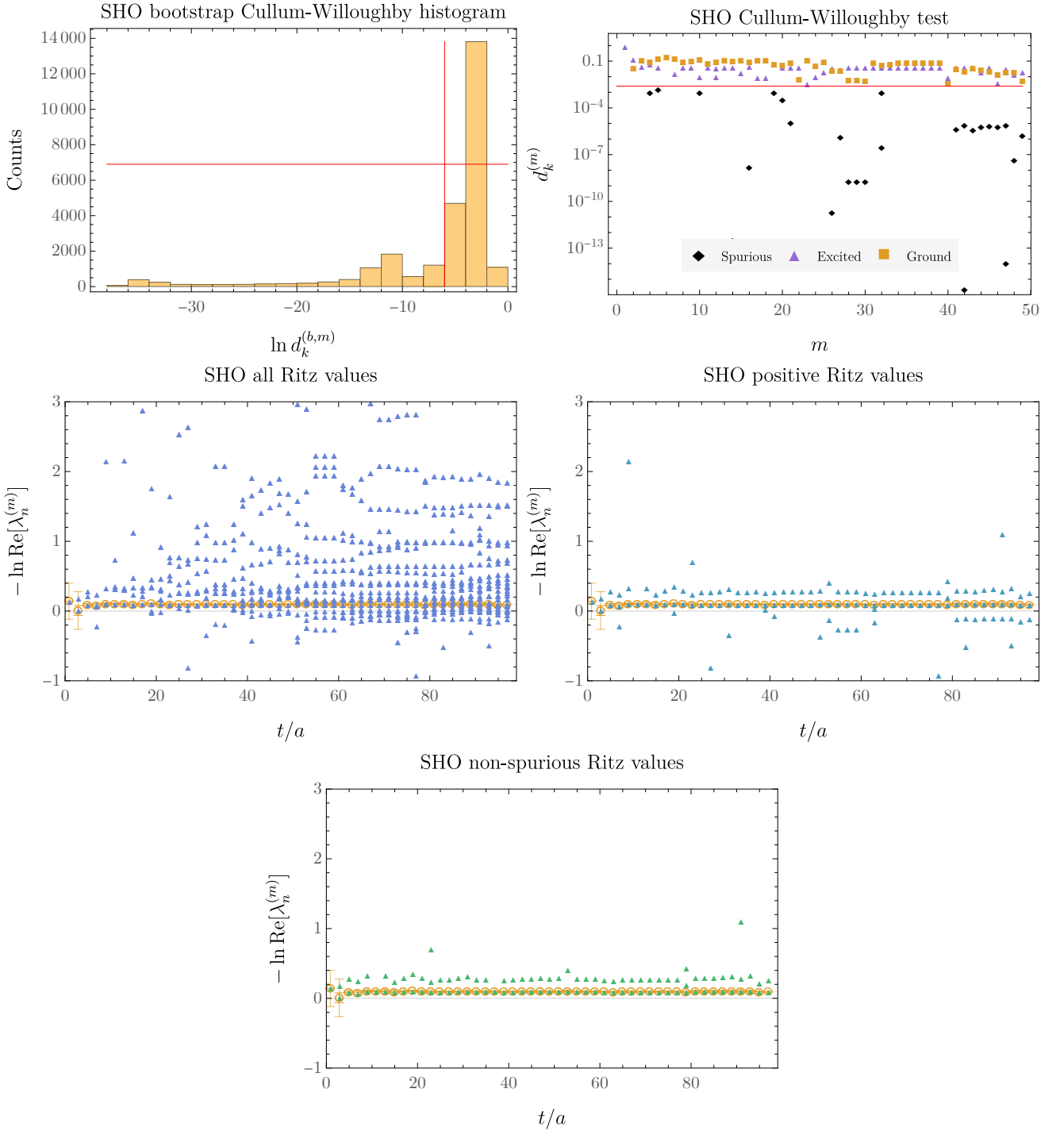


FIG. 6. Summary of the Cullum-Willoughby test used to identify and remove spurious eigenvalues for complex scalar field theory results. The bootstrap histogram of  $\ln d_k^{(b,m)}$  is shown top-left with  $N_\lambda$  computed using  $\Delta = 4$  and  $K_{CW} = 3$  shown as a horizontal red line. The vertical red line shows the corresponding value of  $\ln \varepsilon_{CW}$  computed as described in the text. Top-right, sample mean results for  $d_k^{(m)}$  are shown in comparison with  $\varepsilon_{CW}$  (horizontal red line) with those corresponding to spurious, non-spurious excited-state, and non-spurious ground-state eigenvalues shown as black diamonds, purple triangles, and orange squares, respectively. Middle-left, all of the spurious and non-spurious eigenvalues are shown along with the results for  $E_0^{(m)}$  shown in the main text. Analogous comparisons are shown for all the (spurious and non-spurious) positive eigenvalues, middle-right, and all of the non-spurious eigenvalues (excluding those associated with thermal states), bottom.

further reduce statistical uncertainties in Lanczos results for both energies and residual bounds.

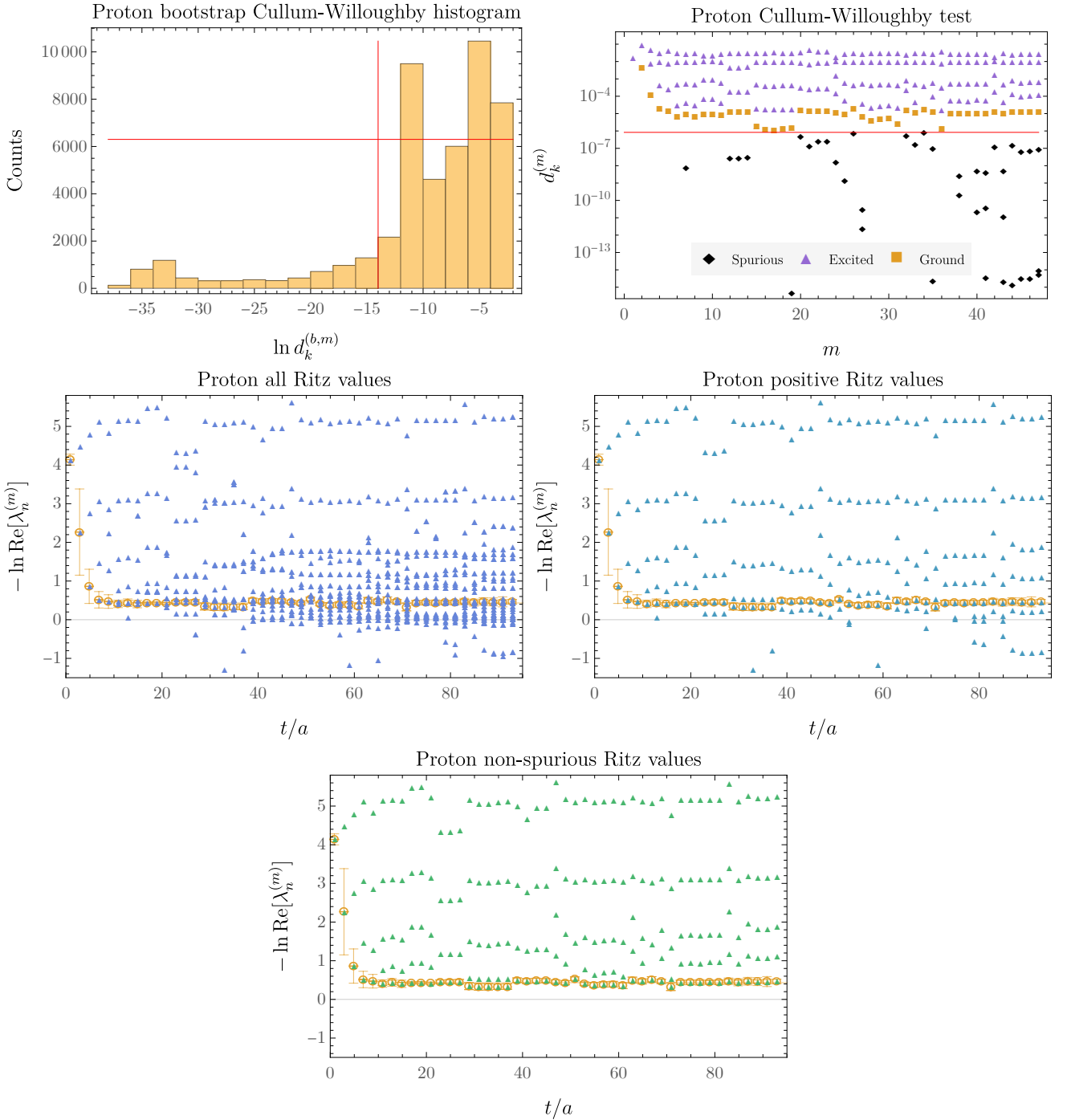


FIG. 7. Summary of the Cullum-Willoughby test for the LQCD proton results in the main text. Details are as in Fig. 6.

To perform fits to Lanczos results, bootstrap covariance matrices are defined as

$$\text{Cov}[E_0^{(m)}, E_0^{(m')}] \equiv \left\langle E_0^{(b,m)} E_0^{(b,m')} \right\rangle_b - \overline{E_0^{(m)} E_0^{(m')}}, \quad (34)$$

where  $\langle \cdot \rangle_b$  denotes a bootstrap sample average and  $\overline{E_0^{(m)}} \equiv \left\langle E_0^{(b,m)} \right\rangle_b$ . The Pearson correlation matrix is

defined as

$$\text{Corr}[E_0^{(m)}, E_0^{(m')}] \equiv \frac{\text{Cov}[E_0^{(m)}, E_0^{(m')}]}{\sqrt{\text{Var}[E_0^{(m)}] \text{Var}[E_0^{(m')}]}, \quad (35)$$

where  $\text{Var}[E_0^{(m)}] \equiv \text{Cov}[E_0^{(m)}, E_0^{(m)}]$ . With these definitions  $\sqrt{\text{Var}[E_0^{(m)}]}$  is found to be of similar magni-

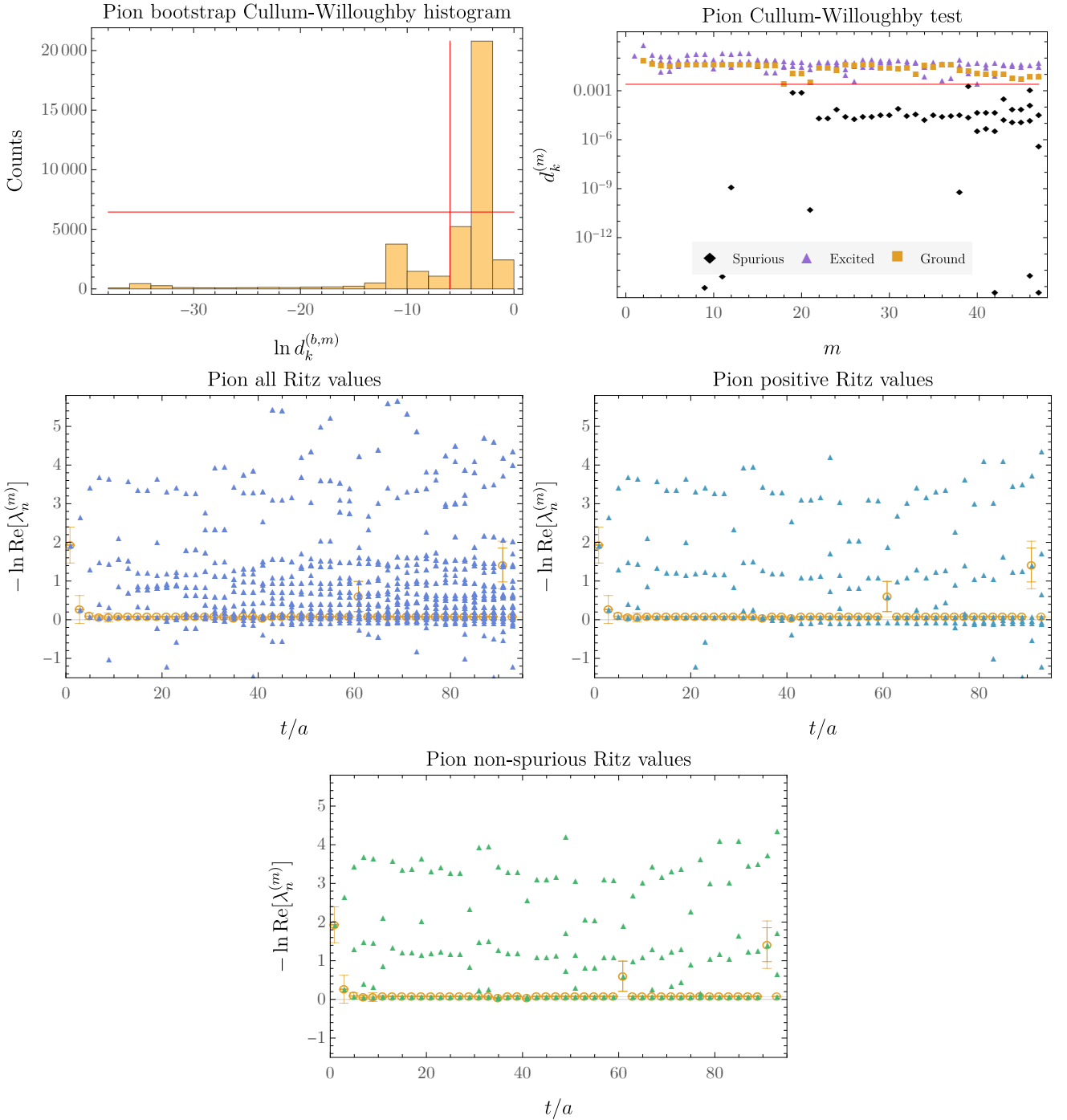


FIG. 8. Summary of the Cullum-Willoughby test for the LQCD pion results in Sec. E. Details are as in Fig. 6.

tude to  $\delta E_0^{(m)}$  in the examples studied here, which suggests that outliers in  $E_0^{(b,m)}$  do not make large contributions  $\text{Cov}[E_0^{(m)}, E_0^{(m')}]$ . Analogous definitions for residual bound results are obtained by replacing  $E_0^{(b,m)}$  and  $E_0^{(b,m')}$  with  $R_0^{(b,m)}$  and  $R_0^{(b,m')}$ .

Define  $m_{\min}$  to be the smallest iteration count where  $|R_0^{(m_{\min})}| < \delta R_0^{(m_{\min})}$  and

$$|E_0^{(m_{\min})} - \text{Median}\{E_0^{(m_{\min})}, \dots, E_0^{((\beta+1)/2)}\}| < \delta E_0^{(m_{\min})},$$

which signals that results have converged within both residual and energy uncertainties.

Before forming the bootstrap covariance matrix and its inverse any  $E_0^{(m')}$  are removed as outliers for which  $E_0^{(m')} - \text{Median}\{E_0^{(m_{\min})}, \dots, E_0^{((\beta+1)/2)}\} \geq 5 \text{Median}\{R_0^{(m_{\min})}, \dots, R_0^{((\beta+1)/2)}\}$ . This can occur in particular if the ground-state eigenvalue was mistakenly

removed as spurious and an excited-state energy was identified as  $E_0^{(m)}$  for this  $m$ . The outlier removal step is relevant in practice for the LQCD pion results in Sec. E with  $m \in O = \{18, 21, 31, 46\}$ , where  $O$  denotes the set of outlier points, and it is irrelevant in practice for the SHO and LQCD proton results presented in the main text. I then invert the energy and residual covariance matrices defined for  $m, m' \in \{m_{\min}, \dots, (\beta + 1)/2\} \setminus O$  where  $O$  is the set of outliers described above. Additional covariance matrix regularization based for example on singular value decomposition (SVD) cuts is not found to be necessary for these examples. Constant fit results and their associated uncertainties define the  $E_0^{\text{Lanczos}}$  results and corresponding residual bounds quoted in the main text.

Example results for the determination of Cullum-Willoughby thresholds and spurious eigenvalue identification for SHO, LQCD proton, and LQCD pion results are shown in Figs. 6-8. It is noteworthy that the gap in  $d_n^{(m)}$  between spurious and non-spurious eigenvalues is not large, and in some cases the non-spurious eigenvalue associated with the ground state is close to the threshold. This means that a small increase in  $K_{\text{CW}}$  can cause the ground-state eigenvalue for a particular Lanczos iteration to be labeled spurious, at which point the largest non-spurious eigenvalue will correspond to an excited-state energy. Conversely, a small decrease in  $K_{\text{CW}}$  can cause a spurious eigenvalue with larger magnitude than  $\lambda_0^{(m)}$  to be labeled non-spurious, at which point an unphysically small value for  $E_0^{(m)}$  will be obtained. Although this can introduce undesirable numerical instabilities to the determinations of  $E_0^{(m)}$  for particular  $m$ , spurious eigenvalues — by their spurious nature — have broadly distributed  $\ln d_n^{(m)}$  that only rarely approach the  $\ln d_n^{(m)}$  of non-spurious eigenvalues. When spurious eigenvalues do have  $\ln d_n^{(m)}$  close to those non-spurious eigenvalues, they are often (although not always) also close in magnitude, and in these cases similar  $E_0^{(m)}$  are obtained regardless of which eigenvalues are labeled spurious. The appearance of such “multiple eigenvalues” is commonplace in applications of Lanczos to finite matrices with floating-point arithmetic [65, 66] and complicates Lanczos determinations of excited-state energies.

To understand whether a small change in  $K_{\text{CW}}$  could lead to a significant change in  $\varepsilon_{\text{CW}}$  and therefore to a change in whether eigenvalues with relatively large magnitudes are labeled as spurious, it is sufficient to examine the bootstrap histogram of  $\ln d_n^{(m)}$ . If  $\varepsilon_{\text{CW}}$  is near the top of a histogram bin that has smaller  $\ln d_n^{(m)}$  than all other bins with greater than  $\varepsilon_{\text{CW}}$  counts, then a small change in  $K_{\text{CW}}$  can cause  $\varepsilon_{\text{CW}}$  to be associated with either this bin or a different bin. In this case, it is worthwhile to study the variation of  $E_0^{(m)}$  results with  $K_{\text{CW}}$  choices that lead to both possibilities. Any significant effects on fit results  $E_0$  and/or  $\delta E_0$  arising from such variations should be considered additional systematic uncertainties. In the examples studied here, varying  $\Delta$  and  $N_{\text{bins}}$  over

the ranges indicated leads to negligible effects, and I do not associate a systematic uncertainty with this variation.

#### D. Oblique Lanczos

A nonsymmetric, or oblique, version of the Lanczos algorithm can be used to compute the eigenvalues of non-Hermitian matrices [67, 68, 74]. Even though the transfer matrix  $T$  can be assumed to be Hermitian for LQCD applications, the oblique Lanczos formalism is needed to describe fermions at non-zero temperature as well as asymmetric correlation functions

$$C_{\chi\psi}(t) \equiv \langle \chi(t)\psi^\dagger(0) \rangle = \langle \chi | T^{t/a} | \psi \rangle + \dots \quad (36)$$

The oblique Lanczos formalism also avoids the complex  $T_{ij}^{(m)}$  that arise in applications of the symmetric Lanczos algorithm to noisy Monte Carlo results and violate the usual assumptions of theoretical Lanczos analyses. Oblique Lanczos therefore provides a theoretically rigorous, as well as more numerically stable, starting point for applying Lanczos in situations when  $T$  is Hermitian but the Hermiticity of  $T^{(m)}$  is broken at finite statistics. All numerical results in this work use the oblique Lanczos algorithm in practice.

The primary difference between oblique and symmetric Lanczos is that the former has distinct Krylov spaces of left- and right-Lanczos vectors. These vectors will be denoted  $\langle w_n |$  and  $|v_n\rangle$  respectively. The first iteration of oblique Lanczos involves the matrix element

$$\alpha_1 \equiv \langle w_1 | T | v_1 \rangle = \frac{\langle \chi | T | \psi \rangle}{\langle \chi | \psi \rangle} = \hat{C}_{\chi\psi}(1), \quad (37)$$

where the last equality shows the connection to the ratio of correlation functions  $\hat{C}_{\chi\psi}(t) \equiv C_{\chi\psi}(t)/C_{\chi\psi}(0)$  and implies that  $m = 1$  results coincide with the effective mass (and symmetric Lanczos). The base cases for other tridiagonal matrix elements defined below are  $\beta_1 = 0$  and  $\gamma_1 = 0$ . The matrix elements needed for a recursive construction of oblique Lanczos that does not explicitly access the Lanczos vectors are

$$\begin{aligned} F_j^k &\equiv \langle w_j | T^k | v_j \rangle, \\ G_j^k &\equiv \langle w_j | T^k | v_{j-1} \rangle, \\ H_j^k &\equiv \langle w_{j-1} | T^k | v_j \rangle. \end{aligned} \quad (38)$$

##### 1. Recursion relations

After the first Lanczos iteration, the residuals for the left- and right-Lanczos vectors are defined by [67, 68, 74]

$$\begin{aligned} |r_{j+1}\rangle &\equiv (T - \alpha_j) |v_j\rangle - \beta_j |v_{j-1}\rangle, \\ \langle s_{j+1}| &\equiv \langle w_j | (T - \alpha_j) - \gamma_j \langle w_{j-1}|. \end{aligned} \quad (39)$$



to the symmetric case, but this sign is cancelled in the recursions for  $\langle w_{k+1} |$  by a corresponding sign change in  $\gamma_k$ . This means that the only difference between applying symmetric and oblique Lanczos to a Hermitian operator  $T$  is that  $T_{ij}^{(m)}$  includes  $\gamma_j = -\beta_j < 0$  when  $\beta_j \gamma_j < 0$ , while symmetric Lanczos has a purely imaginary  $\beta_j$  on both off-diagonals. These two matrices can be related by a change of basis and therefore have identical eigenvalues  $\lambda_n^{(m)}$ . This implies that, with arbitrary-precision arithmetic, applying symmetric Lanczos with  $\beta_j \in \mathbb{C}$  gives identical  $E_n^{(m)}$  as applying oblique Lanczos even at finite statistics when fluctuations lead to negative estimates of squared residual norms.

Round-off errors are quite different when the symmetric and oblique Lanczos algorithms are performed using floating-point arithmetic. Using oblique Lanczos,  $T_k^{(m)}$  is real, and its eigenvalues are therefore either exactly real (at working precision) or come in complex conjugate pairs with non-zero imaginary parts. Using symmetric Lanczos,  $T_k^{(m)}$  is generally a complex symmetric matrix, which can have unpaired eigenvalues that are approximately but not exactly real. Distinguishing these approximately real eigenvalues from pairs of complex conjugate eigenvalues is relatively straightforward for the examples studied here, but it adds additional complications that are unnecessary when using oblique Lanczos.

The convergence of oblique Lanczos for non-Hermitian  $T_k^{(m)}$  is governed by an analog of the KPS bound that was derived by Saad in Ref. [74]. Even for the ground state, the bound depends on the entire spectrum rather than just  $E_0$  and  $Z_0$  as in the Hermitian case. Monotonicity and one-sided variational bounds no longer apply for non-Hermitian  $T_k^{(m)}$ ; results can approach from above or below.

### 3. Residual bound: right Ritz vectors

A bound on the residual norms of Lanczos approximations to  $T|v_j\rangle$  and  $\langle w_i|T$  can be obtained straightforwardly for oblique Lanczos [74]. However, Paige's proof of the eigenvalue-level residual bound [45], Eq. (9), does not apply for non-Hermitian  $T$ . In the remainder of this section, I demonstrate that Paige's proof can be extended to the situation relevant for LQCD in which  $T = T^\dagger$  but  $T_{ij}^{(m)}$  is non-Hermitian due to statistical noise and/or using distinct left- and right-Lanczos vectors.

To obtain a formula for computing the residual norm, first note that the eigenvectors  $s_k^{(m)}$  of  $T_{ij}^{(m)}$  appearing in the eigendecomposition

$$T_{ij}^{(m)} = \sum_k s_{ik}^{(m)} \lambda_k^{(m)} (s^{-1})_{kj}^{(m)}, \quad (54)$$

satisfy the eigenvalue equation

$$\sum_k T_{ik}^{(m)} s_{kj}^{(m)} = s_{ij}^{(m)} \lambda_j^{(m)}, \quad (55)$$

which can be seen by matrix multiplying Eq. (54) by  $s_{jl}^{(m)}$  on the right and relabeling indices. The right Ritz vectors, defined by

$$|y_k^{(m)}\rangle \equiv \sum_i |v_i\rangle s_{ik}^{(m)}, \quad (56)$$

provide the Hilbert-space vectors corresponding to the eigenvectors of  $T_{ij}^{(m)}$ . To make this correspondence precise, define a Hilbert space operator  $T^{(m)}$  by

$$T^{(m)} |v_j\rangle \equiv \sum_i |v_i\rangle T_{ij}^{(m)}. \quad (57)$$

The matrix elements of this operator are given by

$$\begin{aligned} \langle w_i | T^{(m)} |v_j\rangle &= \sum_k \langle w_i | v_k\rangle T_{kj}^{(m)} \\ &= \sum_k \delta_{ik} T_{kj}^{(m)} \\ &= T_{ij}^{(m)}, \end{aligned} \quad (58)$$

and so that the matrix elements of  $T$  and  $T^{(m)}$  between Lanczos vectors are both equal to the tridiagonal matrix elements  $T_{ij}^{(m)}$ . The Ritz vectors therefore satisfy the eigenvalue equation

$$\begin{aligned} T^{(m)} |y_k^{(m)}\rangle &= \sum_i T^{(m)} |v_i\rangle s_{ik}^{(m)} \\ &= \sum_{i,j} |v_j\rangle T_{ji}^{(m)} s_{ik}^{(m)} \\ &= \sum_j |v_j\rangle \lambda_k^{(m)} s_{jk}^{(m)} \\ &= \lambda_k^{(m)} |y_k^{(m)}\rangle. \end{aligned} \quad (59)$$

Next, note that the action of  $T$  is given by Eq. (39) and  $|r_{j+1}\rangle = \rho_{j+1} |v_{j+1}\rangle = \gamma_{j+1} |v_{j+1}\rangle$  as

$$T |v_j\rangle = \alpha_j |v_j\rangle + \beta_j |v_{j-1}\rangle + \gamma_{j+1} |v_{j+1}\rangle. \quad (60)$$

The analogous action of the tridiagonal matrix  $T^{(m)}$  is given directly from Eq. (48) by

$$\begin{aligned} T^{(m)} |v_j\rangle &= \sum_i |v_i\rangle T_{ij}^{(m)} \\ &= \begin{cases} \alpha_j |v_j\rangle + \beta_j |v_{j-1}\rangle + \gamma_{j+1} |v_{j+1}\rangle, & j < m \\ \alpha_j |v_j\rangle + \beta_j |v_{j-1}\rangle, & j = m, \end{cases} \end{aligned} \quad (61)$$

which leads to

$$[T - T^{(m)}] |v_j\rangle = \delta_{jm} \gamma_{m+1} |v_{m+1}\rangle, \quad (62)$$

where  $|v_{m+1}\rangle$  is the Lanczos vector obtained by extending from  $m$  to  $m+1$  steps. The action of  $T - T^{(m)}$  on Ritz

vectors is therefore

$$\begin{aligned} [T - T^{(m)}] \left| y_k^{(m)} \right\rangle &= \sum_j [T - T^{(m)}] |v_j\rangle s_{jk}^{(m)} \\ &= \gamma_{m+1} s_{mk}^{(m)} |v_{m+1}\rangle. \end{aligned} \quad (63)$$

Defining dual right Ritz vectors (which are distinct from the left Ritz vectors introduced below) via the usual Hilbert space adjoint,

$$\left\langle y_k^{(m)} \right| \equiv \left| y_k^{(m)} \right\rangle^\dagger = \sum_i \langle v_i | [s_{ik}^{(m)}]^*, \quad (64)$$

taking the Hermitian conjugate of Eq. (63) gives

$$\left\langle y_k^{(m)} \right| [T - T^{(m)}]^\dagger = \gamma_{m+1} [s_{mk}^{(m)}]^* \langle v_{m+1} |, \quad (65)$$

since the  $\beta_j$  and  $\gamma_j$  are all real.

These ingredients can be used to compute the Ritz vector residual norm, defined by

$$\begin{aligned} R_k^{(m)} &\equiv ||[T - \lambda_k^{(m)}] |y_k^{(m)}\rangle||^2 \\ &= \left\langle y_k^{(m)} \right| [T - \lambda_k^{(m)}]^\dagger [T - \lambda_k^{(m)}] \left| y_k^{(m)} \right\rangle. \end{aligned} \quad (66)$$

Using Eq. (59) and its complex conjugate, the factors of  $\lambda_k^{(m)}$  can be replaced by  $T^{(m)}$ ,

$$R_k^{(m)} = \left\langle y_k^{(m)} \right| [T - T^{(m)}]^\dagger [T - T^{(m)}] \left| y_k^{(m)} \right\rangle. \quad (67)$$

Using Eq. (63) and Eq. (65) then gives

$$R_k^{(m)} = \gamma_{m+1}^2 |s_{mk}^{(m)}|^2 \langle v_{m+1} | v_{m+1} \rangle. \quad (68)$$

This is the oblique Lanczos analog of the right-hand-side of Eq. (9).

#### 4. Residual bound: spectral representation

Paige's proof connecting the residual bound to eigenvalue error bounds [45] can now be applied. The proof requires the assumption that  $T$  is Hermitian even though non-Hermitian  $T_{ij}^{(m)}$  is allowed. Denoting as usual eigenstates of  $T$  by  $|n\rangle$  and their Hermitian conjugates by  $\langle n|$  with normalization  $\langle n|n\rangle = 1$ , the residual norm has a spectral representation,

$$\begin{aligned} R_k^{(m)} &= \left\langle y_k^{(m)} \right| [T - \lambda_k^{(m)}]^\dagger [T - \lambda_k^{(m)}] \left| y_k^{(m)} \right\rangle \\ &= \left\langle y_k^{(m)} \right| [T - \lambda_k^{(m)*}] [T - \lambda_k^{(m)}] \left| y_k^{(m)} \right\rangle \\ &= \sum_n \left\langle y_k^{(m)} \right| T - \lambda_k^{(m)*} \left| n \right\rangle \left\langle n \right| T - \lambda_k^{(m)} \left| y_k^{(m)} \right\rangle \\ &= \sum_n \left\langle y_k^{(m)} \right| \lambda_n - \lambda_k^{(m)*} \left| n \right\rangle \left\langle n \right| \lambda_n - \lambda_k^{(m)} \left| y_k^{(m)} \right\rangle \\ &= \sum_n |\lambda_k^{(m)} - \lambda_n|^2 \left| Z_{kn}^{(m)} \right|^2, \end{aligned} \quad (69)$$

where  $Z_{kn}^{(m)} \equiv \langle n | y_k^{(m)} \rangle$ . Defining

$$\tilde{\lambda}_k^{(m)} \equiv \min_{\lambda \in \{\lambda_n\}} |\lambda_k^{(m)} - \lambda|, \quad (70)$$

where the minimum is over the discrete set of true eigenvalues, i.e.  $\tilde{\lambda}_k^{(m)}$  is the closest true eigenvalue to  $\lambda_k^{(m)}$ , an inequality for  $R_k^{(m)}$  can be derived from Eq. (69) as

$$\begin{aligned} R_k^{(m)} &\geq \sum_n |\lambda_k^{(m)} - \tilde{\lambda}_k^{(m)}|^2 \left| Z_{kn}^{(m)} \right|^2 \\ &= |\lambda_k^{(m)} - \tilde{\lambda}_k^{(m)}|^2 \sum_n \left| Z_{nk}^{(m)} \right|^2, \end{aligned} \quad (71)$$

because  $\tilde{\lambda}_k^{(m)}$  is always nearer or identical to the replaced  $\lambda_n$ . The overlap factor sum can be expressed as

$$\begin{aligned} \sum_n |Z_{kn}^{(m)}|^2 &= \sum_n \left\langle y_k^{(m)} \right| n \rangle \left\langle n \right| y_k^{(m)} \rangle \\ &= \left\langle y_k^{(m)} \right| y_k^{(m)} \rangle. \end{aligned} \quad (72)$$

which allows  $R_k^{(m)}$  to be expressed as

$$\begin{aligned} R_k^{(m)} &\geq |\lambda_k^{(m)} - \tilde{\lambda}_k^{(m)}|^2 \left\langle y_k^{(m)} \right| y_k^{(m)} \rangle \\ &= \min_{\lambda \in \{\lambda_n\}} |\lambda_k^{(m)} - \lambda|^2 \left\langle y_k^{(m)} \right| y_k^{(m)} \rangle. \end{aligned} \quad (73)$$

Combining this with Eq. (68) provides a direct analog of the residual bound, Eq. (9), for oblique Lanczos,

$$\min_{\lambda} |\lambda_k^{(m)} - \lambda|^2 \leq \gamma_{m+1}^2 |s_{mk}^{(m)}|^2 V_k^{(m)}, \quad (74)$$

where

$$\begin{aligned} V_k^{(m)} &\equiv \frac{\langle v_{m+1} | v_{m+1} \rangle}{\left\langle y_k^{(m)} \right| y_k^{(m)} \rangle} \\ &= \frac{\langle v_{m+1} | v_{m+1} \rangle}{\sum_{ij} [s_{ik}^{(m)}]^* \langle v_i | v_j \rangle s_{jk}^{(m)}}. \end{aligned} \quad (75)$$

#### 5. Residual bound: left Ritz vectors

An identical derivation can be performed using the left Ritz vectors

$$\left\langle x_k^{(m)} \right| \equiv \sum_i (s^{-1})_{ki}^{(m)} \langle w_i |, \quad (76)$$

which satisfy

$$\begin{aligned} \left\langle x_k^{(m)} \right| T^{(m)} &= \sum_i (s^{-1})_{ki}^{(m)} \langle w_i | T^{(m)} \\ &= \sum_{ij} (s^{-1})_{ki}^{(m)} T_{ij}^{(m)} \langle w_j | \\ &= \sum_j \lambda_k^{(m)} (s^{-1})_{kj}^{(m)} \langle w_j | \\ &= \lambda_k^{(m)} \left\langle x_k^{(m)} \right|, \end{aligned} \quad (77)$$

and their duals  $|x_k^{(m)}\rangle \equiv \langle x_k^{(m)} |^\dagger$ . Together with

$$\langle w_j | [T - T^{(m)}] = \delta_{jm} \beta_{m+1} \langle w_{m+1} |, \quad (78)$$

the spectral representation for  $\| \langle x_k^{(m)} | [T - \lambda_k^{(m)}] \|^2$  analogous to Eq. (69) can be used to show that

$$\min_{\lambda} |\lambda_k^{(m)} - \lambda|^2 \leq \beta_{m+1}^2 |(s^{-1})_{km}^{(m)}|^2 W_k^{(m)}, \quad (79)$$

where

$$\begin{aligned} W_k^{(m)} &\equiv \frac{\langle w_{m+1} | w_{m+1} \rangle}{\langle x_k^{(m)} | x_k^{(m)} \rangle} \\ &= \frac{\langle w_{m+1} | w_{m+1} \rangle}{\sum_{ij} (s^{-1})_{ki}^{(m)} \langle w_i | w_j \rangle [(s^{-1})_{kj}^{(m)}]^*}. \end{aligned} \quad (80)$$

When  $\langle w_i | = |v_i\rangle^\dagger$ , as for symmetric bosonic correlation functions in the infinite statistics limit, then  $T_{ij}^{(m)}$  is symmetric,  $s_{ij}^{(m)}$  is unitary, and both Eq. (74) and Eq. (79) reduce to Eq. (9). In general, Eq. (74) and Eq. (79) provide rigorous two-sided bounds on the eigenvalue error  $\min_{\lambda} |\lambda_k^{(m)} - \lambda|^2$  that are valid stochastically at finite statistics. Both bounds hold simultaneously, so the more constraining one may be taken.

#### 6. Residual bound: auxiliary recursion relations

To compute (stochastic estimators for) these bounds in practice, it remains to obtain formulae for  $\langle v_i | v_j \rangle$  and  $\langle w_i | w_j \rangle$ . For  $\langle v_i | v_j \rangle$  these can be obtained using recursion relations for

$$\begin{aligned} R_{ij}^k &\equiv \langle v_i | T^k | v_j \rangle = R_{ji}^k, \\ A_j^k &\equiv R_{jj}^k, \end{aligned} \quad (81)$$

The relevant recursions can be derived as in the symmetric case by inserting Eqs. (39)-(40) into Eq. (81). The recursion relation needed to obtain  $R_{i(j+1)}^k$  for  $i \leq j$  is

$$\rho_{j+1} R_{i(j+1)}^k = R_{ij}^{k+1} - \alpha_j R_{ij}^k - \beta_j R_{i(j-1)}^k, \quad (82)$$

and the relation needed for  $A_{j+1}^k = R_{(j+1)(j+1)}^k$  is

$$\begin{aligned} \rho_{j+1}^2 A_{j+1}^k &= A_j^{k+2} - 2\alpha_j A_j^{k+1} + \alpha_j^2 A_j^k + \beta_j^2 A_{j-1}^k \\ &\quad + 2\alpha_j \beta_j R_{j(j-1)}^k - 2\beta_j R_{j(j-1)}^{k+1}. \end{aligned} \quad (83)$$

The analogous set of matrix elements required for  $\langle w_i | w_j \rangle$  is given by

$$\begin{aligned} L_{ij}^k &\equiv \langle w_i | T^k | w_j \rangle = L_{ji}^k, \\ B_j^k &\equiv L_{jj}^k. \end{aligned} \quad (84)$$

The recursion relation needed to obtain  $L_{i(j+1)}^k$  for  $i \leq j$  is

$$\tau_{j+1} L_{i(j+1)}^k = L_{ij}^{k+1} - \alpha_j L_{ij}^k - \gamma_j L_{i(j-1)}^k, \quad (85)$$

and the relation for  $B_{j+1}^k = L_{(j+1)(j+1)}^k$  is

$$\begin{aligned} \tau_{j+1}^2 B_{j+1}^k &= B_j^{k+2} - 2\alpha_j B_j^{k+1} + \alpha_j^2 B_j^k + \gamma_j^2 B_{j-1}^k \\ &\quad + 2\alpha_j \gamma_j R_{j(j-1)}^k - 2\gamma_j R_{j(j-1)}^{k+1}. \end{aligned} \quad (86)$$

The factors of  $V_k^{(m)}$  and  $W_k^{(m)}$  appearing in the oblique Lanczos residual bounds, Eq. (74) and Eq. (79), can be computed straightforwardly from these recursion results,

$$\begin{aligned} V_k^{(m)} &= \frac{A_{m+1}^0}{\sum_{ij} [s_{ik}^{(m)}]^* R_{ij}^0 s_{jk}^{(m)}}, \\ W_k^{(m)} &= \frac{B_{m+1}^0}{\sum_{ij} (s^{-1})_{ki}^{(m)} L_{ij}^0 [(s^{-1})_{kj}^{(m)}]^*}. \end{aligned} \quad (87)$$

### E. Additional numerical results

Pion correlation functions in LQCD have the distinction of not suffering from exponential StN degradation. Lanczos results for the pion mass are shown in comparison with  $E(t)$  and an arccosh effective mass in Fig. 9. A constant fit to  $E_0^{(m)}$  starting when Lanczos results have converged within noise,  $t/a = 7$ , gives  $am_{\pi}^{\text{Lanczos}} = 0.0760(22)$ . Two-state correlation function fits with the same minimum  $t/a = 7$  give  $am_{\pi}^{2\text{-state}} = 0.0781(8)$ . A weighted average of multi-state fits gives  $am_{\pi}^{\text{averaged}} = 0.0783(18)$ . A much higher-statistics calculation using 1024 Gaussian-smearred sources on 2511 gauge-field configurations with an identical action and lattice volume finds  $am_{\pi}^{\text{big}} = 0.0779(5)$  [91]; nearly identical central values are obtained in Refs. [79, 92] while Ref. [78] obtained 0.0766(9). Lanczos, two-state, and model-averaged fit results all agree with  $am_{\pi}^{\text{big}}$  within  $1\sigma$ . Fits to Lanczos residuals over the same range imply a LQCD energy  $E$  satisfies  $a^2 |E - m_{\pi}^{\text{Lanczos}}|^2 < 0.0000(33)$ .

The residuals  $R_0^{(m)}$  are shown for complex scalar field theory, pion, and proton results in Fig. 10. In all cases central values and uncertainties correspond to bootstrap medians and confidence intervals as described in Sec. C.

Correlation matrices  $\text{Corr}[E_0^{(m)}, E_0^{(m')}]$  are shown for SHO, pion, and proton Lanczos results in Fig. 11. Analogous effective mass correlation matrices  $\text{Corr}[E(t), E(t')]$  with  $t = 2m - 1$  and  $t' = 2m' - 1$  are shown for comparison. In both cases, correlations fall off rapidly away from the diagonal  $m = m'$  for all cases studied here. For the SHO, Lanczos correlations decrease faster with  $|m - m'|$  than effective mass correlations. The standard effective mass also shows significant anticorrelations associated with thermal effects that are absent from Lanczos results. For the pion, Lanczos correlations decrease slightly faster with  $|m - m'|$  than standard effective mass correlations, while for the proton Lanczos and standard effective mass correlations show roughly similar decreases with  $|m - m'|$ .

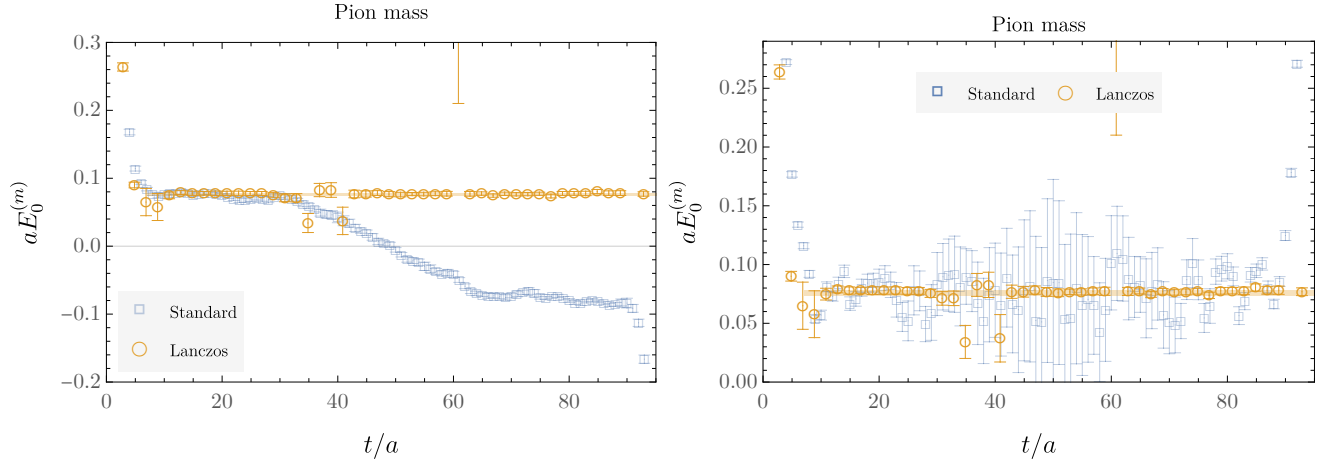


FIG. 9. Left, comparison of the effective mass  $E(t)$  and Lanczos estimator  $E_0^{(m)}$  with  $m = (t/a + 1)/2$  iterations for the pion mass. Right, analogous comparison between  $E_0^{(m)}$  and the standard arccosh effective mass.

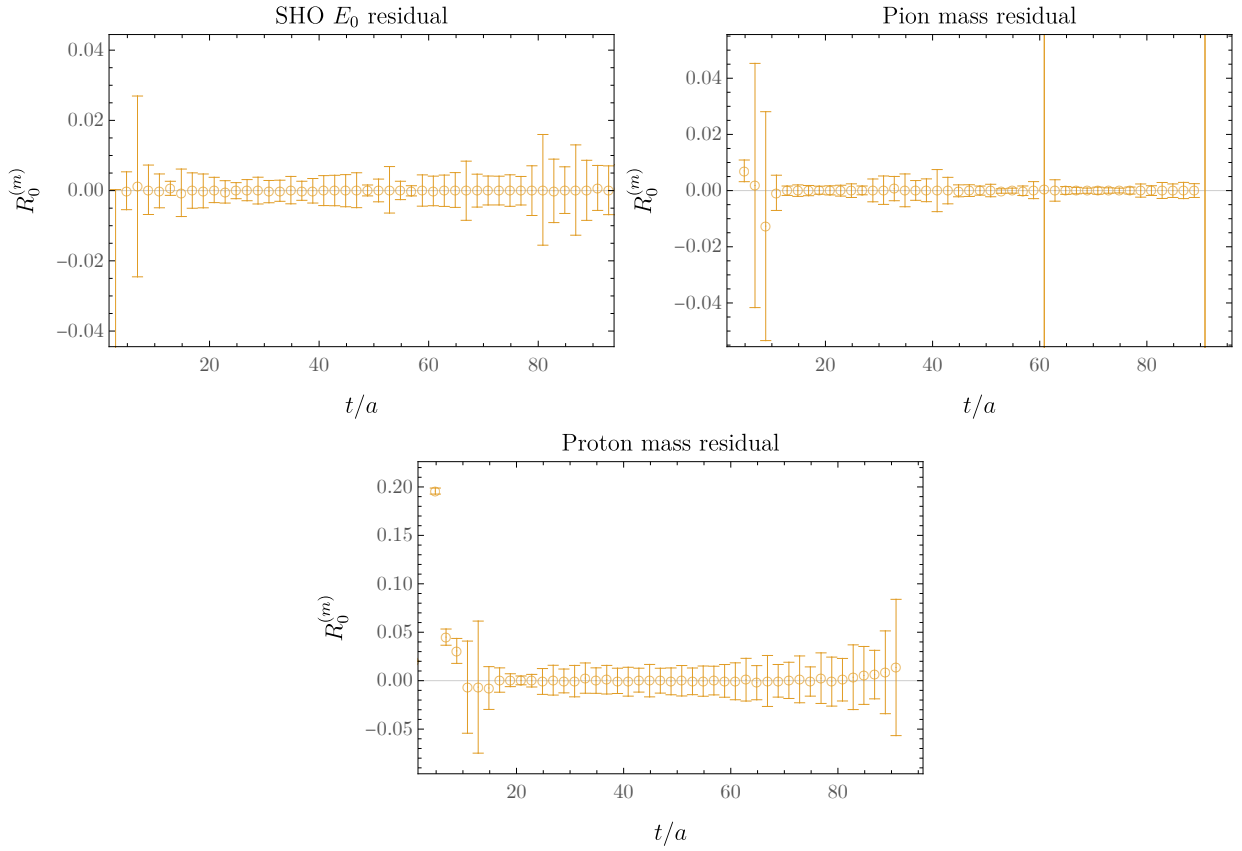


FIG. 10. Residual bounds computed as  $R_0^{(m)} = \min\{V_0^{(m)}, W_0^{(m)}\}$  using the oblique Lanczos formulae, Eq. (74) and Eq. (79), for  $V_0^{(m)}$  and  $W_0^{(m)}$  for the complex scalar field theory boson mass (SHO), LQCD pion mass, and LQCD proton mass as indicated.

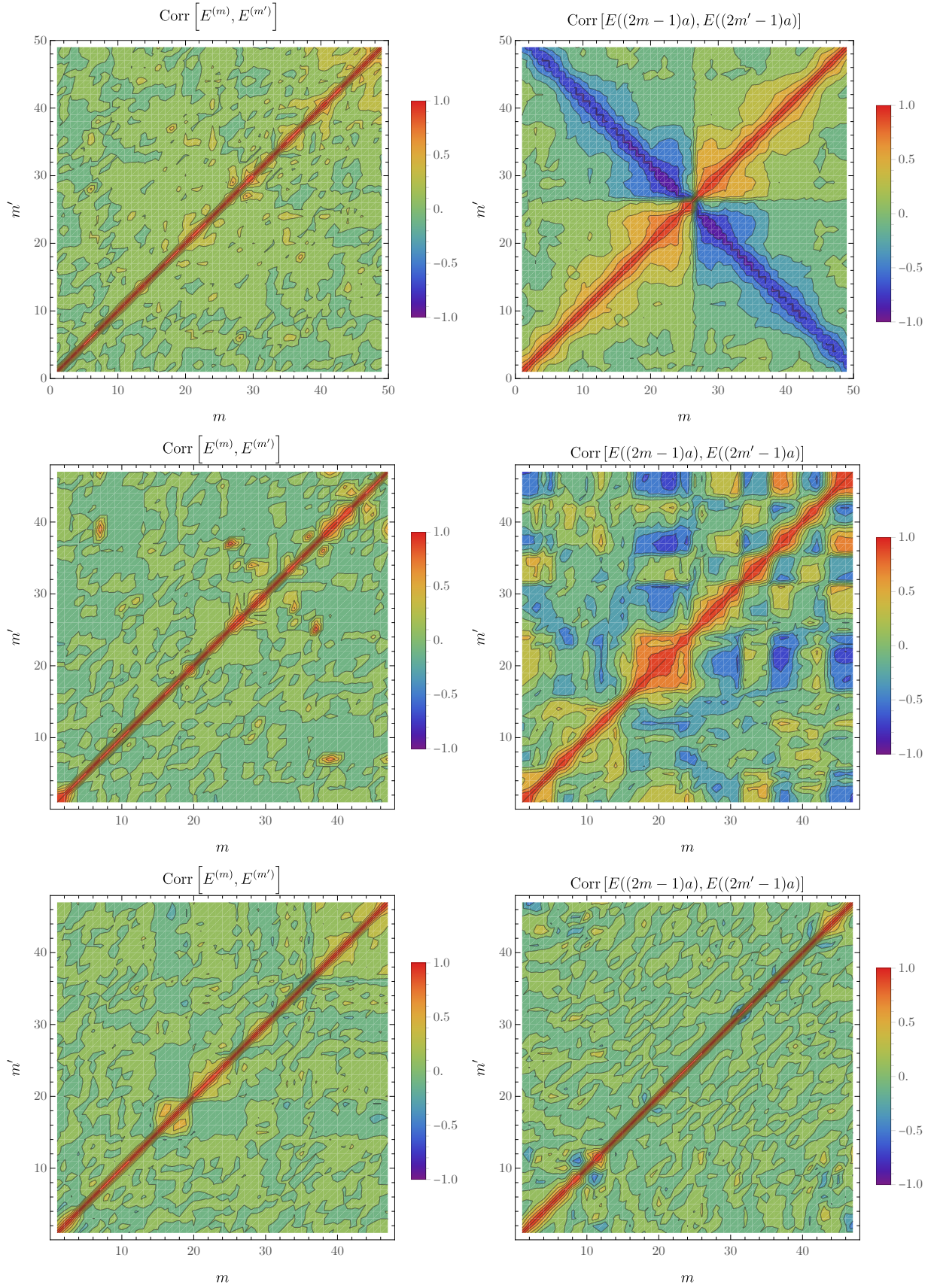


FIG. 11. Correlation matrices defined in Eq. (35) for Lanczos (left) and effective mass (right) results for complex scalar field theory (top), the LQCD pion mass (middle), and the LQCD proton mass (bottom).